NASA TECHNICAL NOTE

NASA TN D-7791

NASA TN D-7791

FLIGHT-PATH AND AIRSPEED CONTROL DURING LANDING APPROACH FOR POWERED-LIFT AIRCRAFT

by James A. Franklin and Robert C. Innis

Ames Research Center

Moffett Field. Calif. 94035

NATIONAL AERONAUTICS AND SPACE ADMINISTRATION • WASHINGTON, D. C. • OCTOBER 1974

TABLE OF CONTENTS

FLIGHT-PATH AND AIRSPEED CONTROL DURING LANDING APPROACH FOR POWERED-LIFT AIRCRAFT

James A. Franklin and Robert C. Innis

Ames Research Center

SUMMARY

Manual control of flight path and airspeed during landing approach has been investigated for powered-lift transport aircraft. An analysis was conducted to identify the behavior of the aircraft which would be potentially significant to the pilot controlling flight path and airspeed during the approach. The response characteristics found to describe the aircraft behavior were (1) the initial flight-path response and flight-path overshoot for a step change in thrust, (2) the steady-state coupling of flight path and airspeed for a step change in thrust, and (3) the sensitivity of airspeed to changes in pitch attitude. The significance of these response characteristics was evaluated by pilots on a large-motion, ground-based simulator at Ames Research Center. Coupling between flight path and airspeed was considered by the pilots to be the dominant influence on handling qualities for the approach task. Results are compared with data obtained from flight tests of three existing powered-lift V/STOL aircraft.

INTRODUCTION

Manual control of STOL transport aircraft operating along steep flight paths is generally more difficult than control of current generation jet transports operating at higher speeds on conventional ILS approach paths. In particular, longitudinal control of STOL aircraft that utilize significant amounts of power to augment aerodynamic lift is adversely affected by low-speed operation, high wing loading, and high inertias typical of the design. Furthermore, operational constraints imposed by airspace, noise, and the time allotted for terminal area operation, by demands for STOL landing field performance and comfortable landing sink rates, and by requirements for adequate operating margins for flight safety are expected to dictate a precision of flight-path and airspeed control for powered-lift aircraft not demanded of conventional jet transports.

This report presents results of an analytical and experimental investigation of flight-path and airspeed control. The study focussed on operation on the glideslope. Problems of controlling large changes in flight path or airspeed associated with transitioning from level flight onto the glideslope or flaring to a landing were not addressed. This report consolidates and extends the work summarized in reference 1, and provides a basis for interpreting the results of reference 1 in terms of the aircraft behavior under pilot control.

Futhermore, the results are related to available flight-test data from V/STOL aircraft.

This report is intended to provide the user with sufficient background information to analyze and make preliminary evaluations of the basic handling qualities of the aircraft for flight-path and airspeed control and to conduct preliminary control system design studies for improving handling qualities. For such purposes, the entire report should be useful: the more casual reader may pass over the details of analysis in section 2 and still have an appreciation of the essential contributions to path and speed control and of the simulation results and flight data.

SECTION 1

BACKGROUND AND REPORT ORGANIZATION

Past experience with several powered-lift aircraft operating along steep approach paths (refs. 2-4) and recent results of ground-based and in-flight simulator evaluations of jet STOL aircraft (refs. 5-9) have emphasized the difficulties of path and speed control which result from

- sluggish flight-path response to attitude changes
- operation on the backside of the drag curve
- large changes in lift and drag with engine power setting
- significant coupling between flight path and airspeed with either attitude or power changes.

Figure 1 illustrates the difficulty of tracking on glideslope with such adverse characteristics. The pilot is forced to make several throttle adjustments to reacquire the glideslope and then does so only with considerable difficulty. Also note the poor speed control. Speed decays after the path is corrected, and the reference approach speed (60 knots) is never reacquired. Time histories that demonstrate the response to attitude and thrust for the STOL aircraft are shown in figure 2. Time histories for a current generation jet transport are included for comparison. The initial change in flight path in response to an abrupt change in pitch attitude (fig. 2(a), constant thrust) is much less for the STOL than for the CTOL aircraft. Furthermore, the direction of the STOL flight-path correction eventually reverses. Flight path is more responsive to a throttle input for the STOL aircraft (fig. 2(b), constant attitude), but the initial correction is partially washed out because of the eventual change in airspeed. The speed change associated with a throttle input is decidedly unconventional in that the airplane decelerates following an increase in power and vice versa.

Such behavior implies that significant demands are placed on the pilot in the way of attention and effort required to control flight-path and speed

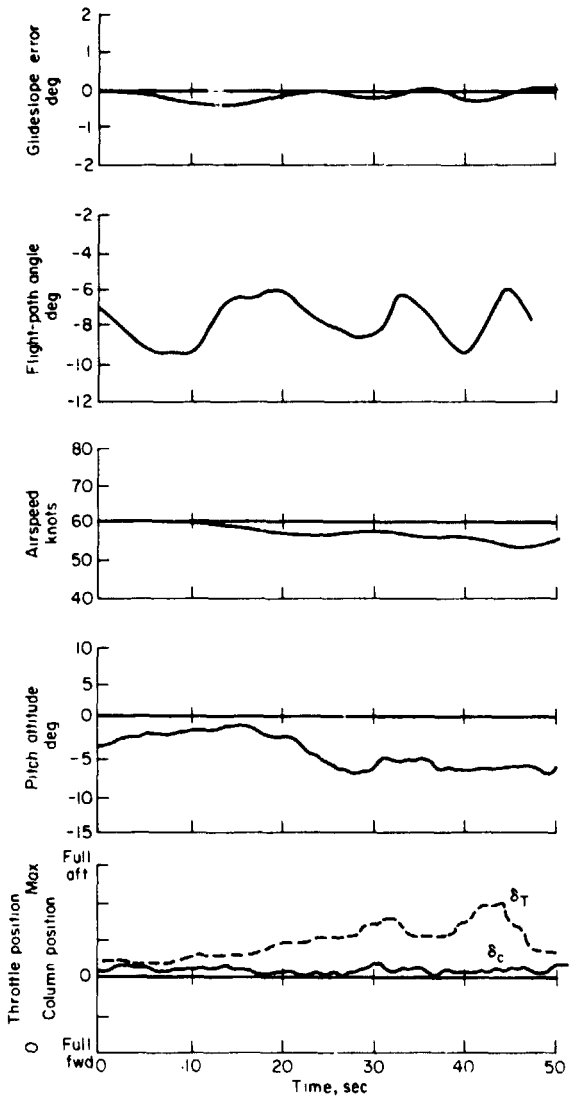

Figure 1.- Example of glide slope tracking for large flight-path/airspeed coupling.

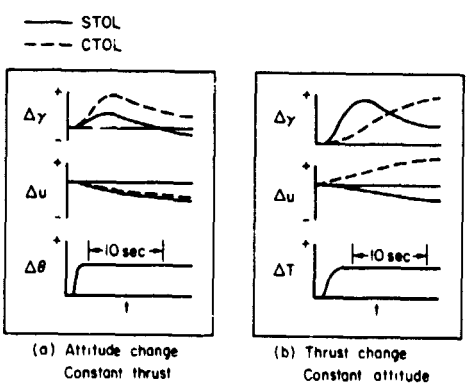

Figure 2.- Flight-path and airspeed response to attitude and thrust (STOL-CTOL comparison).

to achieve acceptable performance during a STOL approach and landing. It thus becomes important to identify the characteristics of the aircraft's behavior which influence the precision with which the pilot can control path and speed on a slow steep approach and the workload associated with the task.

This report is organized as follows. Section 2 presents an analytical description of flight-path and airspeed control. In this analysis, path and speed response to simple inputs through the pilot's primary controls are described. Here the basic response characteristics are discussed and the features important to control precision for the landing approach are identified. So long as the response characteristics are uncomplicated to the pilot and are sufficient to allow him to perform the approach task satisfactorily, the description of the aircraft behavior resulting from these simple, open-loop control applications would provide an adequate basis for analyzing the control task. When the response characteristics are unsatisfactory or when external disturbances such as those imposed by turbulence force the pilot to devote continuous attention to controlling path and speed, the behavior of the aircraft under continuous or closed-loop control by the pilot must be considered. The second step in the analysis defines the characteristics of flight-path and speed response when each is independently controlled by the pilot and, finally, when both are controlled simultaneously. The final step in the analysis is a description of the flight-path and airspeed response characteristics that define the pilot-in-the-loop behavior of the airplane and that are used to structure the experimental program.

Section 3 describes an experimental program devised for a ground-based simulator study of the influence of the individual response characteristics on handling qualities for the STOL approach. Results are presented in terms of pilot ratings and descriptive time histories.

Section 4 compares existing flight data with the results of this simulation. Data from past flight tests which are well tailored for such a comparison are extremely limited; hence the comparison is more qualitative rather than quantitative and conclusive in nature.

SECTION 2

ANALYSIS OF FLIGHT-PATH AND AIRSPEED CONTROL

Flight-Path and Airspeed Response to Thrust and Attitude Control

The pilot's control of flight path and airspeed on the glide slope depends considerably on the ease with which he can make predictable adjustments to the approach path or speed without having to pay excessive attention to the ensuing response or coordinate his controls. The path and speed response of the aircraft to the pilot's control inputs play an important role in that they determine how quickly and predictably the pilot can make a correction in either path or speed without unnecessarily disturbing the other

and how tightly the pilot can control path or speed without having to compensate for deficiencies in the aircraft behavior.

In the discussion which follows, the controls over path and speed used by the pilot are the elevator and engine thrust and the aircraft's response to them is considered. Additional cockpit controls (such as for direct lift or drag) are neither necessary nor desirable because of the increased complexity of the control task and the resulting increase in pilot workload required to coordinate their use. It is well to recognize that the elevator is not normally used to directly control flight path or airspeed but rather to control pitch attitude. Precise control of attitude is essential to establish and hold flight path or airspeed and, in fact, attitude can be used as a command reference by the pilot for path or speed. Consequently, it is appropriate to consider commanded pitch attitude rather than the elevator to be one of the primary path and speed controls.

With pitch attitude tightly controlled, it is shown in appendix A that the response of flight path and airspeed to attitude commands and changes in thrust is described by the equations of motion

$$\begin{bmatrix} s - X_u & -X_\alpha & 0 \\ -Z_u & V_o s - Z_\alpha & 0 \\ 0 & 1 & 1 \end{bmatrix} \begin{Bmatrix} u \\ \alpha \\ \gamma \end{Bmatrix} = \begin{bmatrix} -g \cos \theta_o & X_{\Delta T} \\ V_o s - g \sin \theta_o & Z_{\Delta T} \\ 1 & 0 \end{bmatrix} \begin{Bmatrix} \theta_c \\ \Delta T \end{Bmatrix} \tag{1}$$

The following relationships expressed in the form of transfer functions for response to a particular command may be derived from these equations:

- Response to pitch attitude commands:

  flight path:

$$\left(\frac{\gamma}{\theta_c}\right)_{\theta \to \delta_e} = \frac{A_{\gamma_\theta}(s + 1/T_{\gamma_1})}{s^2 + 2\zeta_\theta \omega_\theta s + \omega_\theta{}^2} \tag{2a}$$

  airspeed:

$$\left(\frac{u}{\theta_c}\right)_{\theta \to \delta_e} = \frac{A_{u_\theta}(s + 1/T_{u_1})}{s^2 + 2\zeta_\theta \omega_\theta s + \omega_\theta{}^2} \tag{2b}$$

- Response to thrust changes:

  flight path:

$$\left(\frac{\gamma}{\Delta T}\right)_{\theta \to \delta_e} = \frac{A_{\gamma_T}(s + 1/T_{\gamma_T})}{s^2 + 2\zeta_\theta \omega_\theta s + \omega_\theta{}^2} \tag{3a}$$

airspeed:

$$\left(\frac{u}{\Delta T}\right)_{\theta \to \delta_e} = \frac{A_{u_T}(s + 1/T_{u_T})}{s^2 + 2\zeta_\theta \omega_\theta s + \omega_\theta{}^2} \tag{3b}$$

The path and speed transfer functions to attitude and thrust in equations (2) and (3) appear in the general form:

$$\frac{\text{response}}{\text{command}} = \frac{A(s + 1/T)}{s^2 + 2\zeta_\theta \omega_\theta s + \omega_\theta{}^2} \tag{4}$$

with the distinguishing features being the gain A, the numerator root 1/T, and the closed-loop phugoid frequency and damping, ω_θ and ζ_θ. The correspondence between these features and a time history of the response to a step command input are shown in figure 3:

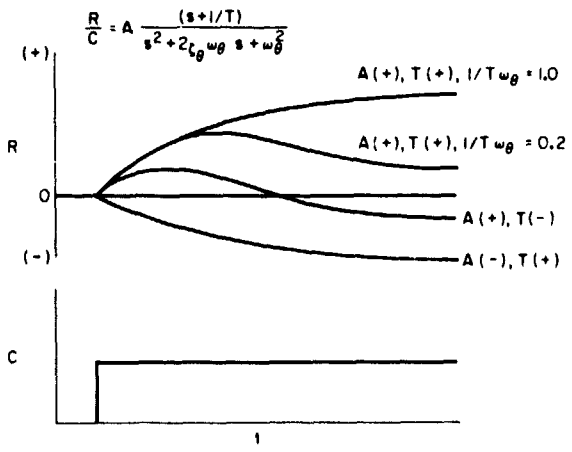

Figure 3.- Examples of time response characteristics.

- The sign of A determines the sign of the initial response.
- The sign of 1/T determines whether the initial and final response are of the same sign.
- The magnitude of A determines how quickly the airplane responds initially.
- The ratio of 1/T to ω_θ determines the amount of overshoot of the response.
- The magnitude of $A/T\omega_\theta{}^2$ determines the magnitude of the steady-state response.

The wide range of response characteristics illustrated by this example is not generally reflected in the individual path and speed responses. Specific behavior for path and speed response is listed in table 1, which shows the contributions of the individual stability derivatives to the transfer function factors in equation (4). The implications of these individual derivatives in the context of each response transfer function are:

- Flight-path response to attitude
  - Initial response is of the same sign as the attitude with slope ($\dot{\gamma}$) scaled by $[(-Z_\alpha + g \sin \theta_o)/V_o]$.

TABLE 1.- CONTRIBUTIONS TO FLIGHT-PATH AND AIRSPEED TRANSFER FUNCTIONS*

Transfer function	A	$\frac{1}{T}$	$2\zeta_\theta\omega_\theta$ or $\left(\frac{1}{T_{\theta_1}} + \frac{1}{T_{\theta_2}}\right)$	ω_θ^2 or $\left(\frac{1}{T_{\theta_1}T_{\theta_2}}\right)$
$\frac{\gamma}{\theta_c}$	$\frac{-Z_\alpha + g \sin\theta_o}{V_o}$	$-X_u + Z_u\left(\frac{X_\alpha - g\cos\theta_o}{Z_\alpha - g\sin\theta_o}\right)$	$-X_u - \frac{Z_\alpha}{V_o}$	$X_u\frac{Z_\alpha}{V_c} - Z_u\frac{X_\alpha}{V_o}$
$\frac{u}{\theta_c}$	$X_\alpha - g\cos\theta_o$	$\frac{g}{V_o}\left(\frac{Z_\alpha\cos\theta_o - X_\alpha\sin\theta_o}{X_\alpha - g\cos\theta_o}\right)$		
$\frac{\gamma}{\Delta T}$	$\frac{-Z_{\Delta T}}{V_o}$	$-X_u + Z_u\frac{X_{\Delta T}}{Z_{\Delta T}}$		
$\frac{u}{\Delta T}$	$X_{\Delta T}$	$\frac{-Z_\alpha}{V_o} + \frac{X_\alpha}{V_o}\frac{Z_{\Delta T}}{X_{\Delta T}}$		

*$X_{\Delta T}$ and $Z_{\Delta T}$ are the longitudinal and vertical axial force derivatives due to thrust resulting from thrust-augmented aerodynamics and direct thrust contributions.

- Numerator root ($1/T_{\gamma_1}$) may be negative[1] for which condition the path response will reverse sign in the steady state.
- Steady-state path change will be less in magnitude than the attitude change ($\gamma/\theta_c < 1$).

- Airspeed response to attitude
  - Sign of the initial response is the same as that of ($X_\alpha - g\cos\theta_o$) or ($-D_\alpha$); hence the normal behavior would be to decelerate for an increase in attitude and vice versa.

---

[1] $1/T_{\gamma_1} < 0$ when $X_\alpha < (X_u/Z_u)(Z_\alpha - g\sin\theta_o) + g\cos\theta_o$
and thus since $X_\alpha = g - D_\alpha$ and $Z_\alpha = -(g/C_L)(C_{L_\alpha} + C_D)$,
$1/T_{\gamma_1} < 0$ when $C_D/C_L < [C_{D_\alpha} - C_L(1 - \cos\theta_o)]/(C_{L_\alpha} + C_L\sin\theta_o + C_D)$
or approximately $C_D/C_L < C_{D_\alpha}/C_{L_\alpha}$.

- Numerator root $(1/T_{u_1})$ is normally positive (unless $D_\alpha < 1$); hence the initial and final responses have the same sign.
- Numerator root is normally larger than the closed-loop phugoid root $(1/T_{u_1}\omega_\theta > 1)$; hence there is no overshoot in the speed response.
- Ratio of speed to path response is determined by gT_{γ_1}.

- Flight-path response to thrust
  - Initial response $(\dot{\gamma})$ scales with $(-Z_{\Delta T}/V_o)$ where an increase in thrust produces an increase in flight-path angle.
  - Sign of the numerator root $(1/T_{\gamma_T})$ is normally positive, but may become negative if $X_{\Delta T}$ has a large enough negative value, which produces a reversal in sign of the steady-state response.
  - Numerator root is typically less than the closed-loop phugoid root $[(1/T_{\gamma_T}\omega_\theta) < 1$ unless $X_{\Delta T}$ is large enough to make $(-X_u + Z_u X_{\Delta T}/Z_{\Delta T}) > \omega_\theta]$; hence there is an overshoot in path response to thrust.
  - Magnitude of the response is determined by $(-Z_{\Delta T}/V_o T_{\gamma_T}\omega_\theta^2)$.

- Airspeed response to thrust
  - Sign and magnitude of the initial response is determined by the sign and magnitude of $X_{\Delta T}$; hence, if the effective thrust turning exceeds 90°, the initial response to an increase in thrust will be a deceleration.
  - Sign of the numerator root $(1/T_{u_T})$ is negative when $0 < X_{\Delta T} < Z_{\Delta T}X_\alpha/Z_\alpha$; hence the speed response may reverse in sign.
  - Ratio of speed to path response is determined by

$$\left(\frac{\Delta u_{ss}}{\Delta \gamma_{ss}}\right)_{\Delta T} = \frac{T_{\gamma_T}\omega_\theta^2}{Z_u/V_o}\left(1 + \frac{1}{T_{\gamma_T}\omega_\theta^2}\frac{Z_\alpha}{V_o}\right) \tag{5}$$

or

$$\left(\frac{\Delta u_{ss}}{\Delta \gamma_{ss}}\right)_{\Delta T} = \frac{(u/\Delta T)_{ss}}{(\gamma/\Delta T)_{ss}} = \left(\frac{A_{u_T}}{T_{u_T}\omega_\theta^2}\right)\left(\frac{T_{\gamma_T}\omega_\theta^2}{A_{\gamma_T}}\right)$$

where the individual terms are defined in table 1.

Figure 2 illustrates path and speed response to attitude and thrust for a jet STOL transport configuration. This example indicates the type of response that might be expected from the foregoing discussion.

Considering the response to an attitude change at constant thrust (fig. 2(a)), the nose-up attitude change produces a typical flight-path response for operation on the backside of the drag curve. The glide path initially becomes more shallow but eventually steepens. Speed response is conventional since the aircraft decelerates following a nose-up change in attitude. For an increase in thrust with attitude held constant (fig. 2(b)), flight path responds quickly and is substantially sustained in the long term. The speed response in this instance is decidedly adverse in that the aircraft decelerates after an increase in thrust.

The response characteristics in this example and in the foregoing discussion important to open-loop control on the glide slope are:

- The initial response that determines how quickly a correction can be initiated,

- The relationship of the long-term response to the short-term response (as indicated by the amount of overshoot and whether the long-term response is in the desired direction) which determines how predictably a correction can be made, and

- The extent of coupling between flight path and airspeed in response to an attitude or thrust change which determines the attention the pilot must direct to the state of the aircraft other than the one he is attempting to control.

These response characteristics determine the manual control technique appropriate to the control of path and speed on the glide slope and the ease with which open-loop corrections to path and speed can be made. As subsequently shown, these characteristics also determine the precision with which path and speed can be controlled closed-loop.

Closed-Loop Control Characteristics

Control technique- To evaluate the closed-loop flight-path and airspeed control characteristics, it is necessary to specify how each particular loop is closed, that is to specify the appropriate control technique adopted by the pilot. The nature of the flight-path response to pitch attitude changes of a powered lift aircraft on a steep, slow landing approach (fig. 2) dictates that attitude should not be used to control flight path, at least not in the long term. The reversal in the path response due to operation on the backside of the drag curve is sufficient reason to reject attitude as a path control (see refs. 10 and 11). On the other hand, speed response to attitude is conventional; for this reason, pitch attitude is considered to be the primary control over speed for this type of aircraft in landing approach operations. Flight path responds as rapidly to thrust as to attitude in the short term and is sustained somewhat in the long term. Therefore, thrust is regarded as the appropriate path control. Since speed response to thrust may be either conventional or unconventional in the short term or long term, thrust is not a desirable speed control.

The foregoing description of the pilot's control technique is intended to apply in a general way. For this purpose, it is quite useful for analysis of closed-loop control of path and speed by the pilot. In fact, the analysis strongly indicates that to control path with attitude and speed with thrust is undesirable. This is not to suggest that the pilot does not adopt alternate methods for short-term control such as coordinating his attitude and thrust controls to initiate a path correction and then separating their use to sort out the path and speed responses in a long-term sense. He also may crossfeed his controls or use only one control to correct from a low-fast or a high-slow condition (ref. 12). The foregoing discussion has simply sought to emphasize that the pilot's general control strategy will be appropriate to this aircraft type as indicated in the previous paragraph. This control technique is assumed in the ensuing analysis.

Closed-loop flight-path control- The elements of closed-loop flight-path control are illustrated in figure 4. The relationship of flight path to thrust is described by the transfer function in equation (3a). Engine thrust response to a throttle command is represented by the second-order dynamic relationship with unity steady-state gain (as shown in the figure). The contribution of the pilot is described by a gain factor, a first-order lead, and an equivalent time delay. This representation of the pilot is a suitable approximation for these analyses. It should not be construed as capable of reproducing every detail of his control activity, as might be observed during closed-loop tracking in flight.

Each contribution of the aircraft, the engine response, and the pilot are considered eventually. First, the closed-loop control of flight path without the effects of engine dynamics or of pilot lead and time delay are considered. Figure 5 is a Bode diagram of the thrust to flight-path transfer function. The frequency axis is normalized by frequency ω_θ to lend more generality to the results. The dominant characteristics of the open-loop transfer function which influence the closed-loop characteristics are frequency $\frac{1}{T_{\gamma_T}}$ which determines the frequency bandwidth of the closed-loop system, and the relationship of the numerator to the denominator roots, $1/T_{\gamma_T}\omega_\theta$, which determines the

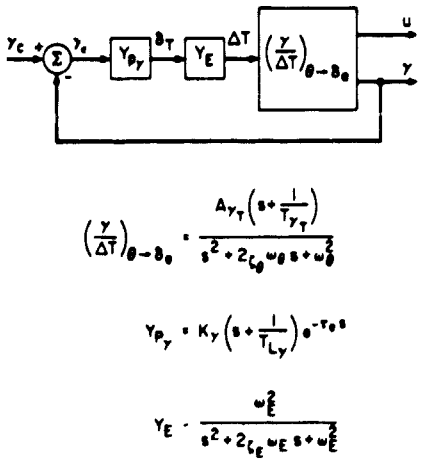

Figure 4.- Block diagram of closed-loop flight-path control.

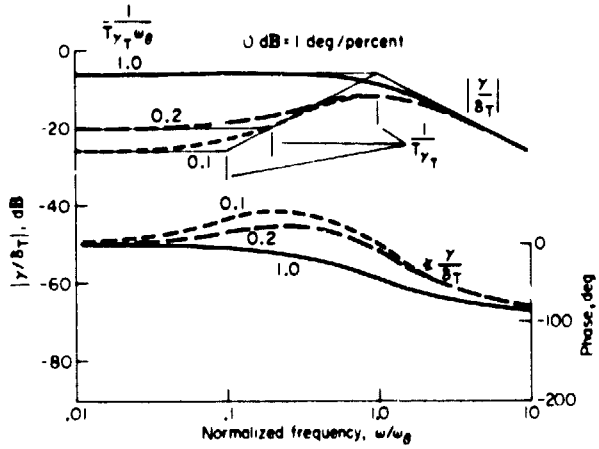

Figure 5.- Oper loop characteristics of flight-path control with thrust.

amount of flight-path overshoot and hence the precision of the long-term or steady-state control of path with thrust. In this case, since there are no constraints on stability, any desired bandwidth may be achieved. In reference 13, a bandwidth corresponding to a gain crossover frequency of 0.5 to 0.7 rad/sec is shown to be desirable for path control. If it is assumed that the gain crossover frequency ω_{co} exceeds ω_θ, the gain for the loop closure can be determined from the accompanying sketch to be

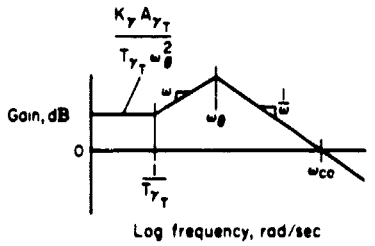

$$K_\gamma \doteq \left(\frac{\omega_{co}}{\omega_\theta}\right)\left(\frac{1}{T_{\gamma_T}\omega_\theta}\right)\left(\frac{T_{\gamma_T}\omega_\theta^2}{A_{\gamma_T}}\right)$$

$$\doteq \frac{\omega_{co}}{-Z_{\Delta T}/V_o} \tag{6}$$

Thus the relationship of path response to command is

$$\left(\frac{\gamma_{ss}}{\gamma_c}\right)_{\substack{\gamma\to\delta_T \\ \theta\to\delta_e}} = \frac{K_\gamma A_{\gamma_T}/T_{\gamma_T}\omega_\theta^2}{1 + K_\gamma A_{\gamma_T}/T_{\gamma_T}\omega_\theta^2}$$

$$= \frac{1}{1 + T_{\gamma_T}\omega_\theta^2/\omega_{co}} \tag{7}$$

Therefore, the lower the crossover frequency and the smaller the ratio of the numerator to denominator root $1/T_{\gamma_T}\omega_\theta$, the greater will be the discrepancy between the final path correction compared to the desired (or commanded) correction.

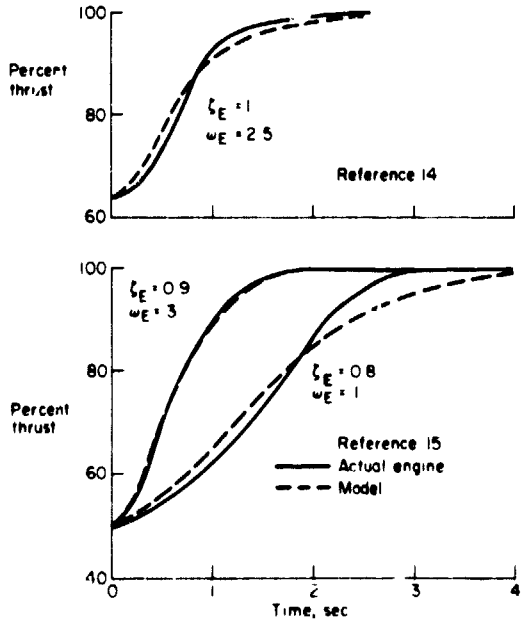

Figure 6.- Comparison of engine response characteristics with second-order dynamic model.

When the contribution of the engine thrust response dynamics is considered, limitations appear on the closed-loop stability of the system. In the second-order model of the engine, the response is assumed to be at least critically damped; for this illustration, the damping ratio is set to unity. Time histories of the engine model are shown in figure 6 and are compared with responses obtained from actual engine response tests reported in references 14 and 15. Note that the S shape of the time history is captured essentially by the second-order response. The Bode plots in figure 5 are repeated in figure 7 with the engine response mode included. Once the separation of the engine and path response modes (ω_E/ω_θ) is less than

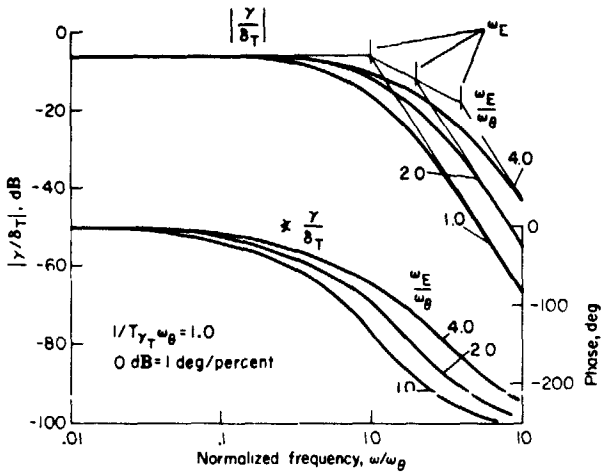

Figure 7.- Influence of engine response on flight-path control with thrust.

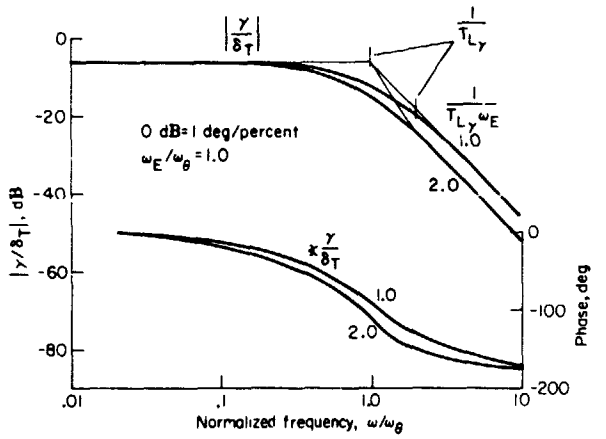

Figure 8.- Influence of pilot compensation on flight-path control with thrust.

a factor of 2, the ability to close the path loop at frequencies much above ω_θ is compromised. In this event, some pilot lead compensation is required to achieve the desired closed-loop bandwidth.

The Bode characteristics (figs. 5 and 7) are based on a normalized frequency scale (ω/ω_θ) and must be related to specific values of ω_θ to indicate the actual limitations on closed loop path control. The relationship for ω_θ^2 (or $1/T_{\theta_1}T_{\theta_2}$ as the case may be) in table 1 suggests a value of ω_θ on the order of 0.3 rad/sec for derivatives typical of STOL aircraft. Such a value approximates ω_θ quite well for the configuration of references 2, 5, 6, and 9 (for these aircraft, ω_θ ranges from 0.25 to 0.31 rad/sec). With ω_θ = 0.3 rad/sec, engine response modes of ω_E = 0.6 rad/sec or less compromise path control unless lead compensation on the order of $1/T_{L_\gamma}\omega_E$ from 1.0 to 2.0 is provided by the pilot (fig. 8). Requirements for pilot-generated lead on the order of T_{L_γ} = 1.0 sec or greater are considered in the literature (e.g., ref. 16) to require excessive pilot effort and attention, with a resulting degradation in handling qualities. Contributions of the pilot equivalent time delay $e^{-\tau_e s}$ in this context seem to be of minor concern in restricting the path-loop closure because of the reasonably wide separation between the equivalent delay factor $1/\tau_e$ and ω_θ ($1/\tau_e\omega_\theta \geq 8$). Restrictions on bandwidth will adversely affect the long-term path response with respect to the command.

Speed response to flight-path control is also of interest in terms of the amount of coupling between the two and the attention required of the pilot for both path and speed control. In this regard, the steady-state speed change in response to a flight-path correction is of particular interest. The relationship $(\Delta u_{ss}/\Delta\gamma_{ss})_{\Delta T}$ in equation (5) indicates contributions from $1/T_{\gamma_T}\omega_\theta$, ω_θ, Z_u, and Z_α. The dominant influence of $1/T_{\gamma_T}\omega_\theta$ on flight-path overshoot in response to thrust was noted previously. The implication of this influence of $1/T_{\gamma_T}\omega_\theta$ (other factors being constant) is that an increase in coupling will cause an increase in flight-path overshoot. Furthermore, the ability to tightly control flight path in the long term will be more difficult with

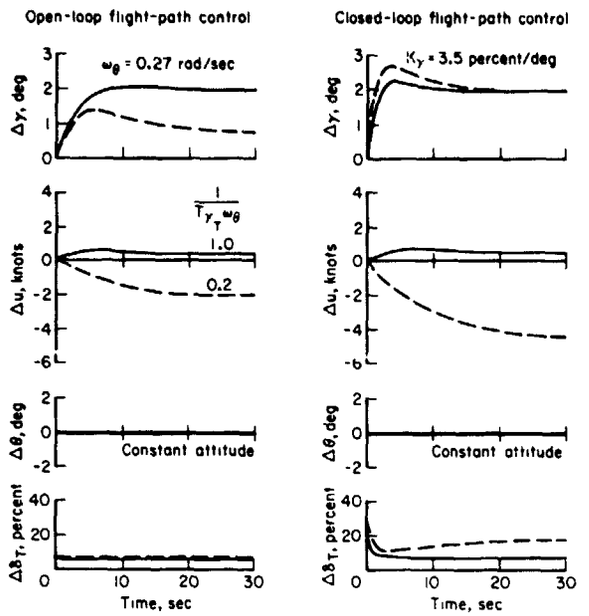

Figure 9.- Example time histories of open- and closed-loop flight-path control with thrust.

increased coupling. Representative time histories of the open-loop and closed-loop path and speed response are shown in figure 9 for configurations with and without flight-path overshoot and path-speed coupling. The open-loop time histories for the uncoupled configuration (represented by $1/T_{\gamma_T}\omega_\theta = 1.0$) indicate that a predictable flight-path correction can be made with a simple throttle application and with essentially no variation in speed. When path and speed are coupled (such as for $1/T_{\gamma_T}\omega_\theta = 0.2$), the initial flight-path response for the same throttle input is still comparable to that for the uncoupled configuration. However, the long-term correction washes out to half the short-term increment. When the flight-path loop is closed (as shown on the right in the figure), the desired long-term path correction can be achieved, but at the expense of increased throttle activity and increased speed excursions.

The interrelationship of the flight-path overshoot and the path-speed coupling characteristics previously noted can be associated with the operation of the aircraft on the backside of the drag curve. Some appreciation of this interrelationship can be gained by considering steady-state flight-path - airspeed plots and their companion lift-drag polars. Figure 10 is an example of these curves for a specific powered-lift concept. Lines of constant attitude and constant flight path are superimposed on the polars. Consider a flight-path change performed by increasing thrust with attitude held constant. The example indicated by the arrow shows an increase in C_L on the polar that accompanies the thrust change, which results in the reduction in speed required to maintain steady 1-g flight as shown on the γ-V plot. If the path correction could be made with no change in C_L and hence at constant speed, this correction would exceed that of the illustrated example for the same thrust increment. The difference in path correction for these two cases arises because of the change in curvature of the polars with increasing C_L for operation on the backside of the drag curve. The point of delineation between the frontside and backside of the drag curve, according to the relationship presented in footnote 1,(p. 7), is defined by $C_{D_\alpha}/C_{L_\alpha} \doteq C_D/C_L$ (the condition for which the local or perturbation lift-drag ratio is equal to the absolute L/D). Any increase in C_L puts the aircraft on the backside of the curve and is accompanied by a proportionally larger increase in C_D so that the total L/D is reduced. This reduction in L/D is the source of the reduced long-term path response. The example in figure 10 is for steady-state conditions. However, so long as $Z_{\Delta T}$, Z_α, and Z_u are held constant,

flight-path overshoot, a characteristic of the transient response, can be inferred from the reduced steady-state path increment associated with the path-speed coupling.

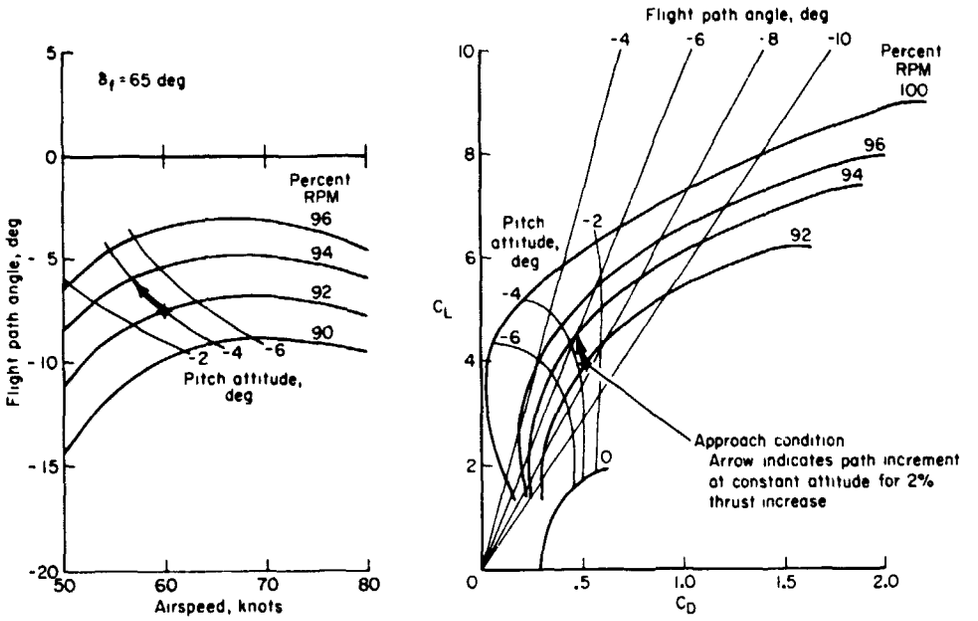

Figure 10.- Variations in flight-path angle-velocity and lift-drag polars with thrust and pitch attitude.

Closed-loop airspeed control- Variations in airspeed which degrade path control are undesirable and make it necessary for the pilot to pay attention to airspeed control during the approach. It was noted in the discussion of control technique that the pilot would be expected to use pitch attitude to control speed. In closing the speed to attitude loop, two types of attitude command control systems that might be available to the pilot must be considered, as well as their implications for closed-loop speed control.

The first type of attitude control system is an attitude command system as shown in figure 11. The speed response to attitude command is given by the transfer function relationship in equation (2b). The pilot is represented in the closed loop by the gain K_u with no lag. The characteristics of the speed loop closure are illustrated in figure 12. In this instance, no constraints are imposed on closed-loop bandwidth by stability. Desired bandwidths for speed control (ref. 12) relate to crossover frequencies on the order of 0.2 to 0.3 rad/sec. If this crossover frequency exceeds ω_θ, the gain for the speed loop closure is approximated by

$$K_u \doteq \frac{(\omega_{co}/\omega_\theta)^2}{A_{u_\theta}/T_{u_1}\omega_\theta^2} \tag{8}$$

which gives a total loop gain of

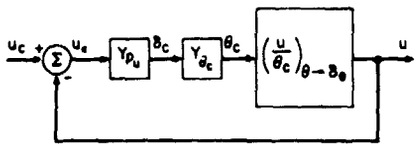

$$\left(\frac{u}{\theta_c}\right)_{\theta-\delta_e} = \frac{A_{u_\theta}\left(s+\frac{1}{T_{u_1}}\right)}{s^2+2\zeta_\theta\omega_\theta s+\omega_\theta^2}$$

$Y_{p_u} = K_u$

$Y_{\theta_c} = 1.0$ Pitch attitude command

$= \frac{T_\theta s+1}{s}$ Pitch rate command

Figure 11.- Block diagram of closed-loop airspeed control.

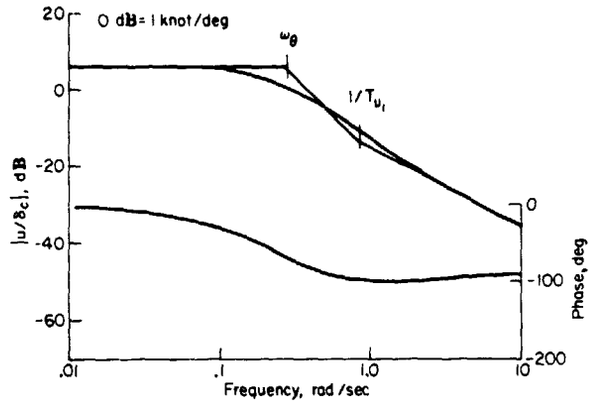

Figure 12.- Airspeed control with pitch attitude (attitude command system).

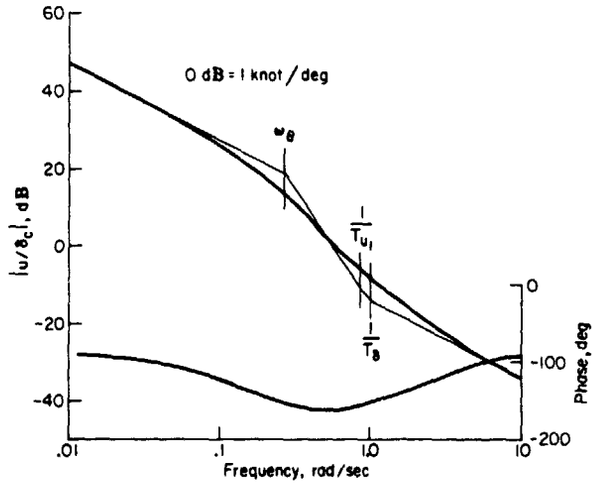

Figure 13.- Airspeed control with pitch attitude (rate command attitude control).

$$\frac{K_u A_{u_\theta}}{T_{u_1}\omega_\theta^2} \doteq \left(\frac{\omega_{co}}{\omega_\theta}\right)^2 \qquad (9)$$

The closed-loop speed response to speed command in the steady state for this transfer function form is

$$\left(\frac{u_{ss}}{u_c}\right)_{\theta\to\delta_e} = \frac{K_u A_{u_\theta}/T_{u_1}\omega_\theta^2}{1 + K_u A_{u_\theta}/T_{u_1}\omega_\theta^2}$$

$$= \frac{1}{(\omega_\theta/\omega_{co})^2 + 1} \qquad (10)$$

For the example shown in figure 12, the ratio of speed response to command is approximately 0.3. Hence, there is a long-term speed standoff error. The extent of the steady-state speed error depends on the relationship of ω_{co} to ω_θ. If the speed error becomes intolerable to the pilot, he will provide an equivalent integral error control to cancel this error.

A pitch attitude control system of the rate command concept also provides a means for eliminating the steady-state speed error so that the pilot need not provide integral control. The rate command system is described in figure 11. This system functions so that a control input commands pitch rate with attitude stabilized when the control input is removed. The numerator time constant should be on the order of a factor of 0.3 to 0.5 of the closed-loop attitude bandwidth for satisfactory pitch rate response sensitivity and minimal overshoot. With this attitude controller, the characteristics of closed-loop speed control are shown in figure 13. The rate command function introduces additional lag at low frequency and, as such, degrades closed-loop stability. If the numerator factors are at high enough frequency, the system becomes unstable for gains that exceed those

for a crossover at ω_θ. However, with the numerator factors as shown in figure 13 and with bandwidths associated with $\omega_{co} = \omega_\theta$, the stability appears to be adequate at the corresponding closed-loop gains. Variations in the numerator factors of either the speed to attitude transfer function or the rate command influence closed-loop stability somewhat at these bandwidths and, in fact, the system may be conditionally stable under some circumstances. The factor $1/T_{u_1}$ is assured to be greater than ω_θ since the likely minimum value of $1/T_{u_1}$ is on the order of $-Z_\alpha/V_o$ and ω_θ will be on the order of $-0.5(X_u + Z_\alpha/V_o)$. The term $1/T_{u_1}$ is shown to be four times ω_θ and would have to be at least ten times ω_θ to reduce the stability margin to unacceptable levels at the closed-loop bandwidth. The pitch rate numerator factor $1/T_\delta$ is also shown to be four times ω_θ - the proper order of magnitude since the attitude stabilization separates ω_θ and the attitude control loop bandwidth by a factor of 10 and the factor $1/T_\delta$ is desired to be about 1/3 to 1/2 the attitude bandwidth. Thus, the general conclusion is that closed-loop speed control evidences no major problems for the bandwidths desired. However, the sensitivity of speed response to attitude changes ($\Delta u_{ss}/\theta_c$) is likely to be of concern to the pilot inasmuch as it determines the gain and the amount of attitude maneuvering required to control speed.

Closed-loop flight-path and airspeed control- When airspeed must be controlled by the pilot, closed-loop control of flight path is described by the block diagram in figure 14. Flight-path response to thrust is represented by the closed-loop transfer function (using the matrix nomenclature for multiloop control of ref. 17):

$$\left(\frac{\gamma}{\Delta T}\right)_{\substack{\theta\to\delta_e \\ u\to\theta_c}} = \frac{N^{\gamma}_{\Delta T} + Y_{p_u} Y_{\theta_c} N^{u}_{\theta_c} \frac{\gamma}{\Delta T}}{\Delta + Y_{p_u} Y_{\theta_c} N^{u}_{\theta_c}} \tag{11}$$

where the numerator is the open-loop flight-path to thrust numerator modified by the speed loop closure and the denominator comprises the factors of the characteristic equation with the speed loop closed. No crossfeed of the throttle to attitude control is included in this analysis. The engine dynamics and pilot model are presented in figure 4 (p. 10).

It is worthwhile to evaluate closed-loop path control without the complicating influences of engine dynamics and pilot compensation and time delays. These contributions

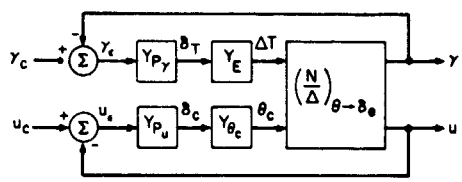

$$\left(\frac{\gamma}{\Delta T}\right)_{\substack{\theta\to\delta_e \\ u\to\theta_c}} = \frac{N^{\gamma}_{\Delta T} + Y_{P_u} Y_{\theta_c} N^{u}_{\theta_c} \frac{\gamma}{\Delta T}}{\Delta + Y_{P_u} Y_{\theta_c} N^{u}_{\theta_c}}$$

$$N^{\gamma}_{\Delta T} = A_{\gamma_T}\left(s + \frac{1}{T_{\gamma_T}}\right) \qquad Y_{P_\gamma} = K_\gamma \left(s + \frac{1}{T_{L_\gamma}}\right) e^{-\tau_\epsilon s}$$

$$N^{u}_{\theta_c} = \omega_{u_\theta}\left(s + \frac{1}{T_{u_1}}\right) \qquad Y_{P_u} = K_u$$

$$N^{u}_{\theta_c}\frac{\gamma}{\Delta T} = \begin{vmatrix} -g\cos\theta_o & -X_\alpha & X_{\Delta T} \\ V_o s - g\sin\theta_o & V_o s - Z_\alpha & Z_{\Delta T} \\ 1 & 1 & 0 \end{vmatrix} = A_{u_\gamma} \qquad Y_{\theta_c} = \begin{cases} 1.0 & \text{Attitude command} \\ \dfrac{T_R s + 1}{s} & \text{Rate command} \end{cases}$$

$$Y_E = \frac{\omega_E^2}{s^2 + 2\zeta_E \omega_E s + \omega_E^2}$$

Figure 14.- Block diagram of closed-loop flight-path and airspeed control.

are assessed after the simpler example is considered. The denominator roots that result from the speed loop closure depend on whether attitude was controlled by an attitude or rate command system. Table 2 presents examples of both cases. For the attitude command system, the denominator is represented by a complex pair of roots with frequency somewhat greater than ω_θ. For the rate command system, the same complex roots exist and, in addition, there is a first-order subsidence.

TABLE 2.- EXAMPLES OF FLIGHT-PATH/THRUST TRANSFER FUNCTIONS

WITH SPEED LOOP CLOSED

$$\left(\frac{\gamma}{\Delta T}\right)_{\substack{\theta \to \delta_e \\ u \to \theta_c}} = \frac{N^{\gamma}_{\Delta T} + Y_{p_u} Y_{\theta_c} N^{u}_{\theta_c} N^{\gamma}_{\Delta T}}{\Delta + Y_{p_u} Y_{\theta_c} N^{u}_{\theta_c}}$$

Speed loop closed around attitude command	Speed loop closed around rate command
Numerator:	Numerator:
$A_{\gamma_T}\left(s + \frac{1}{T_{\gamma_T}}\right) + K_u A_{u\gamma}$	$A_{\gamma_T}\left(s + \frac{1}{T_{\gamma_T}}\right) + K_u A_{u\gamma}\left(\frac{T_\delta s + 1}{s}\right)$
or	or
$A_{\gamma_T}\left(s + \frac{1}{T'_{\gamma_T}}\right)$	$\frac{A_{\gamma_T}}{s}\left(s^2 + 2\zeta'_\gamma \omega'_\gamma s + \omega'^2_\gamma\right)$
Denominator:	Denominator:
$s^2 + 2\zeta_\theta \omega_\theta s + \omega_\theta^2 + K_u A_{u_\theta}\left(s + \frac{1}{T_{u_1}}\right)$	$s^2 + 2\zeta_\theta \omega_\theta s + \omega_\theta^2 + K_u A_{u_\theta}\left(\frac{T_\delta s + 1}{s}\right)\left(s + \frac{1}{T_{u_1}}\right)$
or	or
$\left(s^2 + 2\zeta'_\theta \omega'_\theta s + \omega'^2_\theta\right)$	$\left(\frac{s + 1/T'_{u_1}}{s}\right)\left(s^2 + 2\zeta'_\theta \omega'_\theta s + \omega'^2_\theta\right)$

A key factor in determining whether good closed-loop control of path is possible is the location of the numerator roots. As with the denominator, the nature of these roots depends on the form of attitude control. The numerator for the attitude command system is a first-order factor while the numerator for the rate command system has two first-order factors. For the attitude command system, the numerator gain factor is

$$A_{\gamma_T} = \frac{-Z_{\Delta T}}{V_o} \tag{12}$$

and the time constant is

$$\frac{1}{T'_{\gamma_T}} = \frac{1}{T_{\gamma_T}} + \frac{K_u A_{u\gamma}}{A_{\gamma_T}}$$

$$= -X_u + Z_u \frac{X_{\Delta T}}{Z_{\Delta T}} + K_u \left[X_\alpha - g \cos \theta_o - \frac{X_{\Delta T}}{Z_{\Delta T}} (Z_\alpha - g \sin \theta_o) \right] \tag{13}$$

The two factors that provide the most variability in sign and magnitude of the time constant are the speed loop gain K_u and the effective thrust turning $X_{\Delta T}/Z_{\Delta T}$. The sign of K_u is negative for speed stabilization under most circumstances, while $X_{\Delta T}/Z_{\Delta T}$ can be either positive or negative depending on whether the thrust turning exceeds 90°. Figure 15 illustrates the contribution to the numerator root of these two factors for values of X_u, Z_u, X_α, and Z_α typical of a powered lift aircraft with an 3810 N/m^2 (80 lb/ft^2) wing loading flying a 6° glide slope at 75 knots. Values of K_u, assuming $\omega_{co} \doteq \omega_\theta$, are $K_u \doteq 1/(\Delta u_{ss}/\theta_c)$ and generally range from -0.3° to -1.0°/knot. The intercepts of the constant $X_{\Delta T}/Z_{\Delta T}$ lines with the ordinate indicate the value of the open-loop path to thrust numerator root. Note that as this root shifts to higher frequencies speed is more tightly controlled.

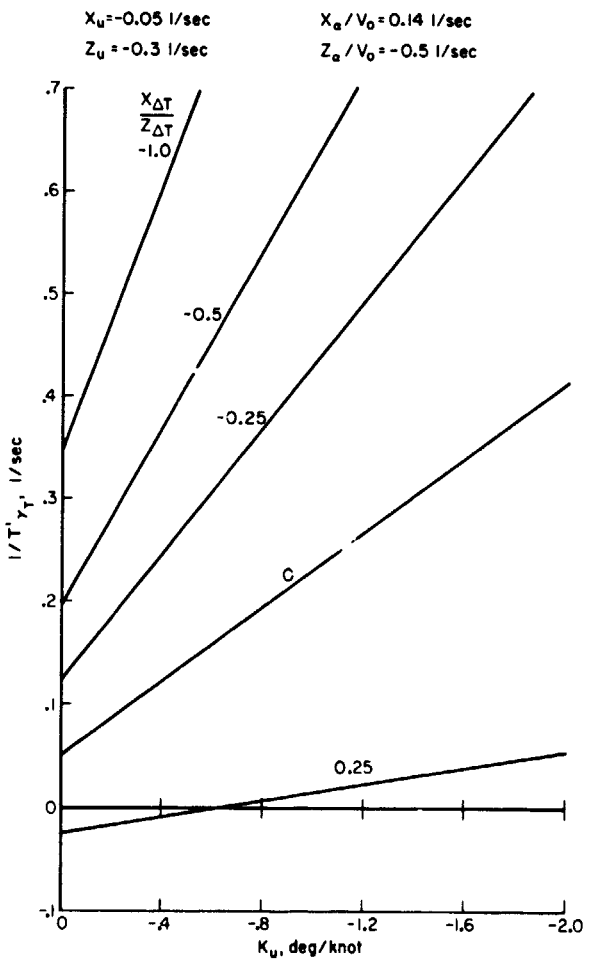

Figure 15.- Contributions to closed-loop flight-path to thrust numerator (attitude command system).

For the rate command system, the numerator gain factor is

$$A_{\gamma_T} = \frac{-Z_{\Delta T}}{V_o}$$

The damping factor is

$$2\zeta'_\gamma\omega'_\gamma = \frac{1}{T_{\gamma_T}} - K_u T_\delta \frac{A_{u\gamma}}{A_{\gamma_T}}$$

$$= -X_u + Z_u \frac{X_{\Delta T}}{Z_{\Delta T}} + K_u T_\delta \left[X_\alpha - g \cos\theta_o - \frac{X_{\Delta T}}{Z_{\Delta T}} (Z_\alpha - g \sin\theta_o) \right] \tag{14}$$

and the natural frequency is

$$\omega'_\gamma = \sqrt{K_u \frac{A_{u\gamma}}{A_{\gamma T}}}$$

$$= \sqrt{K_u \left[X_\alpha - g \cos\theta_o - \frac{X_{\Delta T}}{Z_{\Delta T}} (Z_\alpha - g \sin\theta_o) \right]} \tag{15}$$

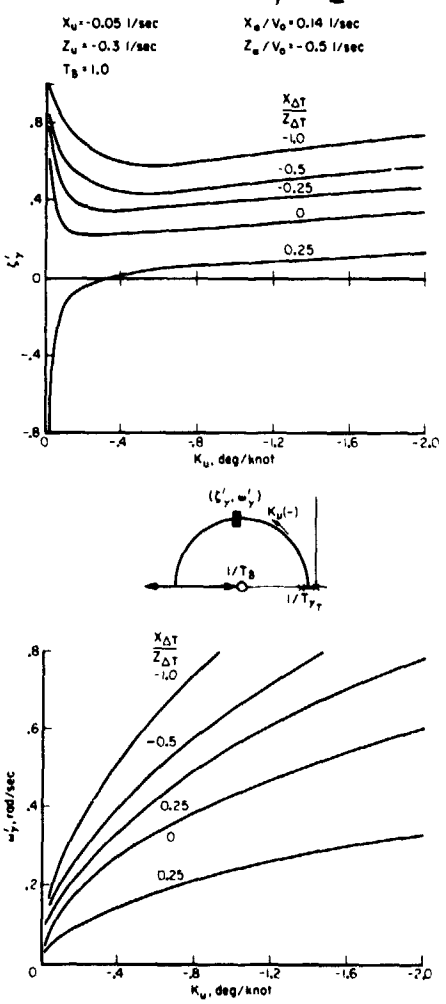

Figure 16.- Contributions to closed-loop flight-path to thrust numerator (rate command system).

Contributions of the speed loop gain and effective thrust turning to the damping ratio and natural frequency are shown in figure 16. For speed loop control gains from -0.3° to -1.0°/knot, the damping ratio is essentially a function of $X_{\Delta T}/Z_{\Delta T}$ and decreases with increased thrust turning. The frequency ω'_γ, a function of both K_u and $X_{\Delta T}/Z_{\Delta T}$, increases as speed is controlled more tightly and decreases with increased thrust turning.

Characteristics of flight-path control with airspeed controlled through the attitude command system are shown in the Bode plot in figure 17. The significant characteristics are the closed-loop frequency ω_θ' and the ratio of the numerator root to this frequency $1/T'_{\gamma_T}\omega'_\theta$. This ratio can be defined from equations (8) and (13) and the vehicle characteristics noted in figure 15 by

$$\frac{1}{T'_{\gamma_T}\omega'_\theta} = \frac{\frac{1}{T_{\gamma_T}} + \left(\frac{0.5 X_{\Delta T}/Z_{\Delta T} - 0.18}{\Delta u_{ss}/\theta_c} \right)}{1.4\ \omega_\theta} \tag{16}$$

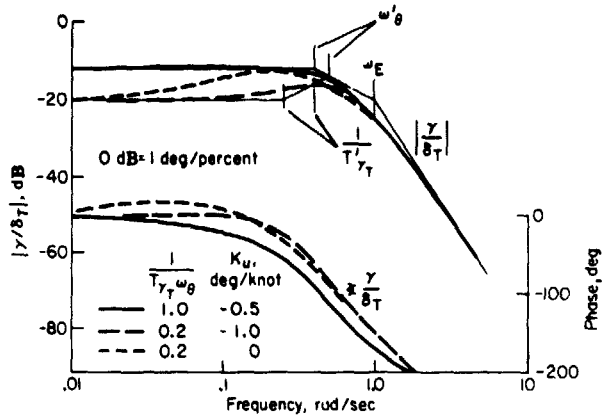

Figure 17.- Flight-path control with thrust with airspeed control by pitch attitude (attitude command system).

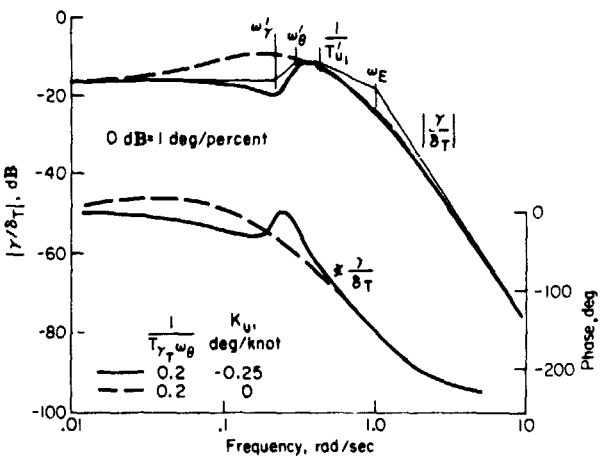

Figure 18.- Flight-path control with thrust with airspeed control by pitch attitude (rate command attitude control system).

since

$$\omega_\theta'^2 = \omega_\theta^2 + K_u\omega_\theta^2\left(\frac{A_{u_\theta}}{T_{u_1}\omega_\theta^2}\right)$$

In figure 17, the range of $1/T'_{\gamma_T}\omega'_\theta$ corresponds to $-0.4 < X_{\Delta T}/Z_{\Delta T} < 0.1$. and $\Delta u_{ss}/\theta_c = -2.0$ knots/deg. The speed loop closure tends to diminish the amount of overshoot in the path response for $1/T_{\gamma_T}\omega_\theta = 0.2$. Lags introduced into the control loop by the engine dynamic response reduce the path control bandwidth essentially to the same extent noted in figure 7 (p. 12)

Flight-path control characteristics for the rate command attitude control are shown in figure 18. This Bode plot differs somewhat from that in figure 17 in that the numerator is a second-order factor while the denominator has first- and second-order factors. Some overshoot in the path response is still indicated by the peak in the Bode plot near 0.3 to 0.4 rad/sec although it is less than the comparable open-loop case. The bandwidth of the path control is determined to some extent by $1/T'_{u_T}$. The degrading influences of engine dynamics are similar to those previously noted in figure 17.

A time history of the open- and closed-loop path and speed response and the corresponding throttle and attitude control activity are shown in figure 19 for two different sets of dynamic characteristics. The uncoupled configuration ($1/T_{\gamma_T}\omega_\theta = 1$) provides good flight-path response to a step throttle input with little control activity required to regulate speed. The coupled configuration ($1/T_{\gamma_T}\omega_\theta = 0.2$) exhibits reasonable path response but requires more throttle activity for the same flight-path correction. It also requires that speed be controlled with attitude to obtain this behavior. The amount of attitude control required depends on the extent of path-speed coupling $(\Delta u_{ss}/\Delta\gamma_{ss})_{\Delta T}$. Examples of these two configurations without speed control are shown in figure 9 (p. 13).

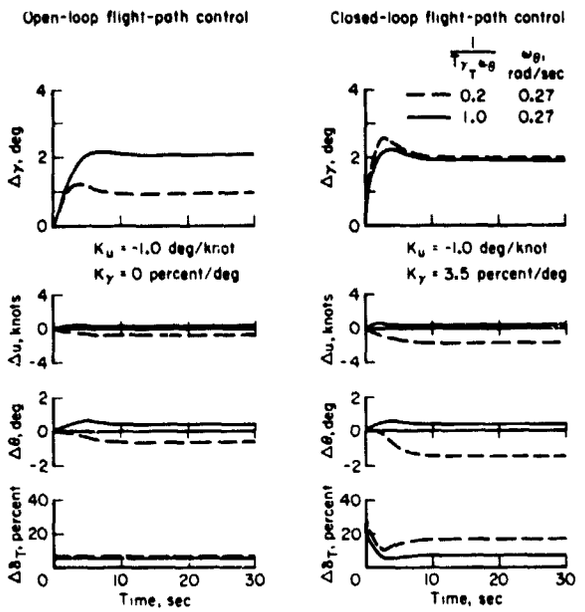

Figure 19.- Time histories of response for a flight-path correction (speed loop closed).

Summary of closed-loop control characteristics- The foregoing discussion described the contributions that influence closed-loop flight path and airspeed control. In summary, the important factors are

- The bandwidth of path response to thrust as determined by ω_θ
- The relationship of the steady-state path response to the commanded path correction as influenced by $1/T_{\gamma_T}\omega_\theta$
- The amount of speed variation that accompanies a path correction (defined by eq. (5))
- The sensitivity of airspeed to variation in attitude, $\Delta u_{ss}/\theta_c$
- The overshoot and long-term stability of closed-loop flight-path control (airspeed loop closed) as influenced by the effective thrust turning $X_{\Delta T}/Z_{\Delta T}$ (also $1/T_{\gamma_T}\omega_\theta$) and by the pilot's speed control gain $K_u = 1/(\Delta u_{ss}/\theta_c)$.

These factors are important in determining how quickly a flight-path correction can be initiated, how predictable the correction is to the pilot, the attention he must devote to path and speed control, the extent to which he must continuously control path and speed closed-loop, and his ability to achieve the precision of control required for the landing approach.

Response Characteristics for Experimental Evaluation

Closed-loop flight-path and airspeed control ultimately depend on and can be quantified by closed-loop bandwidth, stability margin, the ratio of the final response to the command input, the number of control loops involved, and the control activity in each. While these characteristics can be readily determined analytically, they are difficult to specify or identify experimentally. Fortunately, the factors that have a dominant influence on closed-loop control of path and speed are either directly identifiable or are implicit in the open-loop path and speed response to attitude and thrust. Thus, it is these open-loop characteristics around which an experimental handling qualities evaluation is best structured.

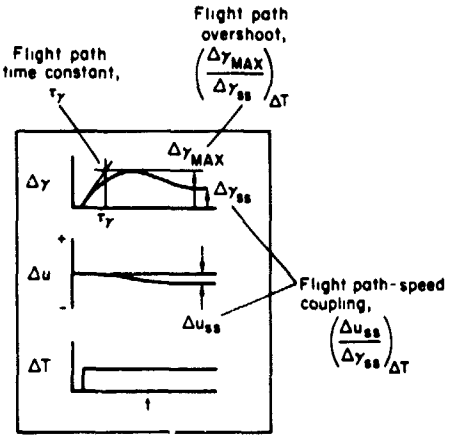

Figure 20.- Characteristics of response of flight path and airspeed to thrust.

The particular open-loop response characteristics to thrust changes are illustrated in figure 20:

- initial flight-path response represented by the time constant τ_γ
- flight-path overshoot represented by $(\Delta\gamma_{max}/\Delta\gamma_{ss})_{\Delta T}$ and
- coupling of flight path and airspeed represented by $(\Delta u_{ss}/\Delta\gamma_{ss})_{\Delta T}$.

Although not shown in figure 20, the sensitivity of airspeed to attitude commands, $\Delta u_{ss}/\theta_c$, is also important.

Derivation of response characteristics- The analytical basis for deriving the four response characteristics noted above is described in the material that follows. Contributions of the aircraft configuration and operating condition on these characteristics are also noted.

The path response time constant, τ_γ, is defined for a step thrust change by

$$\tau_\gamma = \frac{\Delta\gamma_{max}}{\dot{\gamma}}$$

$$= \left(\frac{\Delta\gamma_{max}}{\Delta\gamma_{ss}}\right)_{\Delta T}\left(\frac{\Delta\gamma_{ss}}{\dot{\gamma}}\right)$$

where $\dot{\gamma}$ is defined at $t = 0$, that is, $\dot{\gamma} = -Z_{\Delta T}\Delta T/V_o$:

$$\frac{\Delta\gamma_{ss}}{\dot{\gamma}} = \frac{(-Z_{\Delta T}\Delta T/V_o)\,[1/T_{\gamma_T}\omega_\theta{}^2]}{(-Z_{\Delta T}\Delta T/V_o)}$$

$$= \frac{1}{T_{\gamma_T}\omega_\theta{}^2}$$

and thus

$$\tau_\gamma = \left(\frac{\Delta\gamma_{max}}{\Delta\gamma_{ss}}\right)_{\Delta T}\left(\frac{1}{T_{\gamma_T}\omega_\theta{}^2}\right) \tag{17}$$

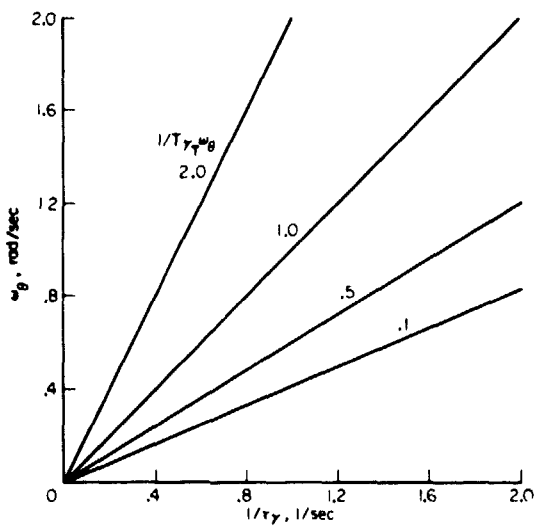

Figure 21.- Relationship between τ_γ and ω_θ.

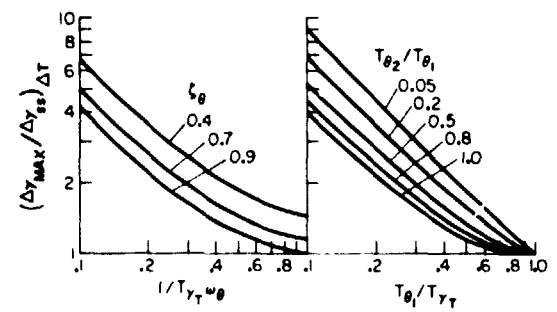

Figure 22.- Contributions to flight-path overshoot ratio.

Therefore, the initial time response depends on both the ratio $1/T_{\gamma_T}\omega_\theta$, which defines the path overshoot characteristics, and the characteristic frequency ω_θ. Figure 21 illustrates these relationships. Note that ω_θ and the inverse time constant $1/\tau_\gamma$ are linearly related for any $1/T_{\gamma_T}\omega_\theta$.

Figure 22 shows the contributions of the transfer function parameters to the amount of flight-path overshoot for a step thrust change. Whether the characteristic roots of the flight-path response are described by $(s^2 + 2\zeta_\theta\omega_\theta s + \omega_\theta{}^2)$ or by $(s + 1/T_{\theta_1})(s + 1/T_{\theta_2})$, the significant contribution is the ratio of the numerator root, $1/T_{\gamma_T}$, to the lowest frequency characteristic root ω_θ or $1/T_{\theta_1}$. Less important is the damping ratio ζ_θ (particularly since ζ_θ tends to be greater than 0.8 for most attitude loop closures) or the ratio of $1/T_{\theta_1}$ to $1/T_{\theta_2}$ [which can fall between the extremes $X_u/(Z_\alpha/V_o) = 0.1$ when $X_\alpha = 0$ and 1.0 when $(X_u + Z_\alpha/V_o)^2 = (4/V_o)(X_uZ_\alpha - X_\alpha Z_u)$]. The amount of overshoot can vary approximately by a factor of 5 when the parameters $1/T_{\gamma_T}\omega_\theta$ or $T_{\theta_1}/T_{\gamma_T}$ vary from 0.1 to 1.0.

The coupling of flight path and airspeed was defined previously in equation (5) as

$$\left(\frac{\Delta u_{ss}}{\Delta \gamma_{ss}}\right)_{\Delta T} = \frac{T_{\gamma_T}\omega_\theta^2}{Z_u/V_o}\left[1 + \left(\frac{1}{T_{\gamma_T}\omega_\theta^2}\right)\frac{Z_\alpha}{V_o}\right]$$

which is a function of $1/T_{\gamma_T}\omega_\theta$ and ω_θ, both of which help to define $(\Delta\gamma_{max}/\Delta\gamma_{ss})_{\Delta T}$ and τ_γ, and also the linear perturbation derivatives Z_u and Z_α. Hence the extent that flight-path speed coupling can vary independently of the flight-path response to thrust is determined by the magnitude of the Z-axis derivatives due to speed and angle of attack.

Speed sensitivity to attitude changes is simply the steady-state magnitude in equation (2), that is,

$$\frac{\Delta u_{ss}}{\theta_c} = \frac{A_{u_\theta}}{T_{u_1}\omega_\theta^2}$$

$$= \frac{g}{V_o}\left(\frac{Z_\alpha \cos\theta_o - X_\alpha \sin\theta_o}{\omega_\theta^2}\right) \qquad (18)$$

with the definitions of the individual terms as in table 1. If $X_\alpha = 0$ ($D_\alpha = g$) so that $\omega_\theta^2 = X_u Z_\alpha / V_o$, then $\Delta u_{ss}/\theta_c = g/X_u$. Speed response to attitude may also be related to the slope of the flight-path versus airspeed curve ($d\gamma/dV$) at a particular trim condition. If the trim pitch attitude is sufficiently small that $\cos\theta_o = 1$ and $(X_\alpha/Z_\alpha)\sin\theta_o << 1$, $(X_u/Z_u)\sin\theta_o << 1$, $(g/Z_\alpha)\sin\theta_o << 1$ then

$$\frac{\Delta u_{ss}}{\theta_c} \doteq \frac{-1}{(1/gT_{\gamma_1}) + (Z_u/Z_\alpha)}$$

$$\doteq \frac{1}{(d\gamma/dV) - (Z_u/Z_\alpha)} \qquad (19)$$

Contributions of aircraft configuration- The contributions to the flight-path and speed control characteristics (shown, respectively, in fig. 22 and eqs. (5), (17), and (18)) are defined in terms of the aircraft X- and Z-axis (or drag and lift) derivatives due to speed, angle of attack, and thrust. Reference 18 shows that these derivatives may be described in terms of the vehicle configurations and flight condition, that is,

X_u axial velocity damping; a function of drag coefficient, trim airspeed and wing loading (may be augmented by autospeed control)

X_α drag due to lift; a function of trim airspeed, wing loading, and induced drag

Z_u vertical force coupling with axial velocity; a function of trim airspeed

Z_α vertical velocity damping; a function of lift-curve slope, trim airspeed, and wing loading

$\frac{X_{\Delta T}}{Z_{\Delta T}}$ effective thrust line inclination $\theta_T = \cot^{-1}(-X_{\Delta T}/Z_{\Delta T})$

These characteristics are determined for all practical purposes by the flight condition at which the aircraft is being operated, by its wing loading, and by the efficiency of its high lift system. Thus, when landing field length (approach speed), cruise Mach number (wing loading), and high lift system design are selected, the behavior of the aircraft as it appears to the pilot during the approach and landing will be essentially determined.

SECTION 3

REVIEW OF SIMULATION RESULTS

Description of Simulation

A ground-based flight simulation of a powered-lift jet STOL aircraft was used as a basis for pilot evaluation of the flight-path and airspeed response characteristics described previously The simulation facility was the Flight Simulator for Advanced Aircraft (FSAA) at Ames Research Center a large-motion facility with a high-resolution visual display (ref. 19). The simulation was based on the NASA/DITC Augmentor Wing Research Aircraft, a modified de Havilland of Canada C-8A Buffalo airframe that incorporates an augmentor flap system to generate high lift coefficients for high wing loading STOL operation and deflected hot thrust for operation on steep flight paths. The aircraft is described in reference 20. Figure 23 presents three views of the aircraft. Figure 24 shows the cockpit interior and control arrangement of the simulator. A real-time digital model of the nonlinear aerodynamics and flight-control system of the aircraft were programmed as described in reference 21. Reference 14 presents the static aerodynamic characteristics as derived from model

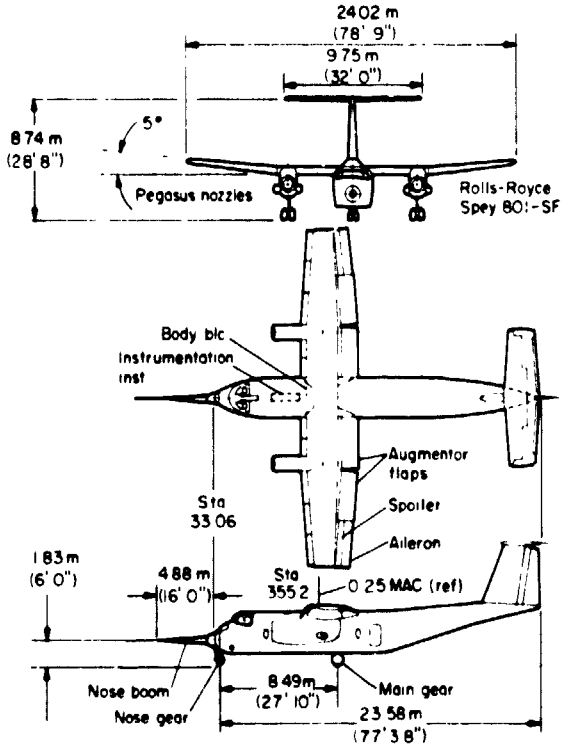

Figure 23.- Augmentor wing research aircraft.

(a) Instrument panel.

(b) Controls.

Figure 24.- Cockpit arrangement of the simulator.

tests of the vehicle in the Ames 40- by 80-Foot Wind Tunnel. Rotary derivatives were estimated by use of jet flap theory where appropriate. Supporting data for these derivatives are unpublished although the models themselves appear in reference 14. Jet engine acceleration/deceleration characteristics were based on the thrust transients of reference 14. Equivalent response parameters appropriate for the engine model are $\zeta_E = 1.0$ and $\omega_E = 2.5$ rad/sec

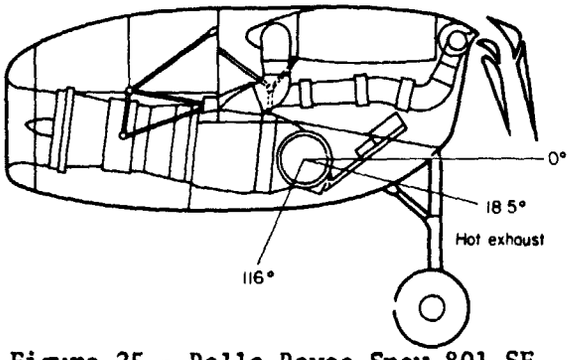

Figure 25.- Rolls Royce Spey 801 SF engine and Pegasus nozzle arrangement.

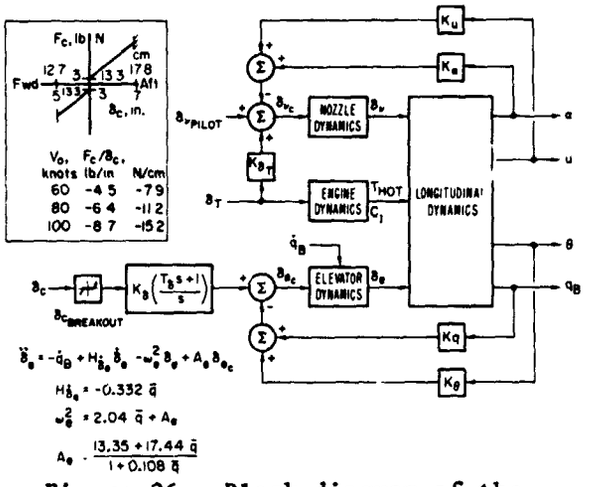

Figure 26.- Block diagram of the longitudinal control system.

The longitudinal flight-control system provided pitch axis command augmentation and alteration of the longitudinal force characteristics by use of vectored thrust. The elevator was mechanically driven through a spring tab system. Augmentation commands were provided by an electro-hydraulic actuator operating in series with the control column inputs of the pilot. Longitudinal force control was achieved by vectoring the hot thrust of the engines about a trim position deflected 90° to the aircraft waterline in response to commands based on errors in airspeed, angle of attack, and throttle position. For thrust vectoring of ±15° about the 90° trim condition, effective alteration of the basic X_u, X_α, and X_{δ_T} derivatives of the aircraft was possible without any significant contribution to the Z-axis force characteristics. Figure 25 shows the orientation of the hot exhaust nozzles for thrust vectoring. Figure 26 is a block diagram of the longitudinal control system. A description of the basic Augmentor Wing Aircraft, in terms of its stability derivatives, characteristic modes, pertinent transfer function numerator factors, and transient response characteristics, is provided in table 3. The dynamics of the elevator-spring tab system are documented in figure 26.

Test Configurations

Flight-path and airspeed control were evaluated using throttle for flight-path control and attitude for speed control as described on page 9. Variations in each of the path and speed response characteristics previously described were achieved by varying the longitudinal force characteristics X_u, X_α, and $X_{\delta_T}/Z_{\delta_T}$ (or θ_T). The contributions of these derivatives are shown in

TABLE 3.- AUGMENTOR WING AIRCRAFT LONGITUDINAL DYNAMICS - LANDING APPROACH CONDITION

Flight-loading conditions	
V_o = 60 knots	C_j = 0.45
γ = -7.5°	GW = 178 kN (40,000 lb)
α = 2.74°	I_y = 280,000 kg-m^2 (207,000 slug-ft^2)
δ_f = 65°	X_{cg} = 29.2 percent of mean aerodynamic chord
δ_ν = 90°	S_w = 80.4 m^2 (865 ft^2)
T_{hot} = 28.4 kN (6380 lb)	$\bar{c}$ = 3.8 m (12.4 ft)

Stability derivatives (body axis)	Response characteristics
X_u = -0.052 1/sec	ζ_p = 0.15
X_α/V_o = 0.14 1/sec	ω_p = 0.22 rad/sec
$X_{\dot{\alpha}}/V_o$ = 0.0011	$1/T_{sp_1}$ = 0.62 rad/sec
X_q/V_o = 0.0025	$1/T_{sp_2}$ = 1.2 rad/sec
X_{δ_e}/V_o = -0.0034 1/sec	$1/T_{\theta_1}$ = 0.18 rad/sec
X_{δ_ν}/V_o = -0.0485 1/sec	$1/T_{\theta_2}$ = 0.37 rad/sec
$X_{\Delta T}/V_o$ = -0.000051 1/sec/%	$1/T_{u_1}$ = 0.84 rad/sec
Z_u = -0.29 1/sec	$1/T_{\gamma_1}$ = -0.06 rad/sec
Z_α/V_o = -0.52 1/sec	$1/T_{u_T}$ = 5.94 rad/sec
$Z_{\dot{\alpha}}/V_o$ = -0.0156	$1/T_{\gamma_T}$ = 0.049 rad/sec
Z_q/V_o = -0.0344	F_c/a_z = 254 N/g (57.2 lb/g)
Z_{δ_e}/V_o = -0.049 1/sec	$\ddot{\theta}/\delta_c$ = 0.028 rad/sec^2/cm (0.07 rad/sec^2/in.)
Z_{δ_ν}/V_o = 0	τ_γ = 1.56 sec
$Z_{\Delta T}/V_o$ = -0.0024 1/sec/%	$(\Delta\gamma_{max}/\Delta\gamma_{ss})_{\Delta T}$ = 2.4
M_u = 0.0017 rad/m/sec (0.00051 rad/ft/sec)	$(\Delta u_{ss}/\Delta\gamma_{ss})_{\Delta T}$ = -3.45 knots/deg
M_α = -0.3 rad/sec^2/rad	$\Delta u_{ss}/\Delta\theta$ = -2.2 knots/deg
$M_{\dot{\alpha}}$ = -0.42 1/sec	
M_q = -0.93 1/sec	
M_{δ_e} = -1.2 rad/sec^2/rad	
M_{δ_ν} = -0.074 rad/sec^2/rad	
$M_{\Delta T}$ = 0.00028 rad/sec^2/%	

figures 27 and 28. Effects of variation in thrust inclination (θ_T) and drag due to lift (X_α) are shown in figure 27 for characteristics otherwise representative of the basic aircraft. Figure 28 shows the influence of axial damping (X_u) combined with thrust inclination. Table 4 summarizes the significant interaction of these derivatives with the response characteristics.

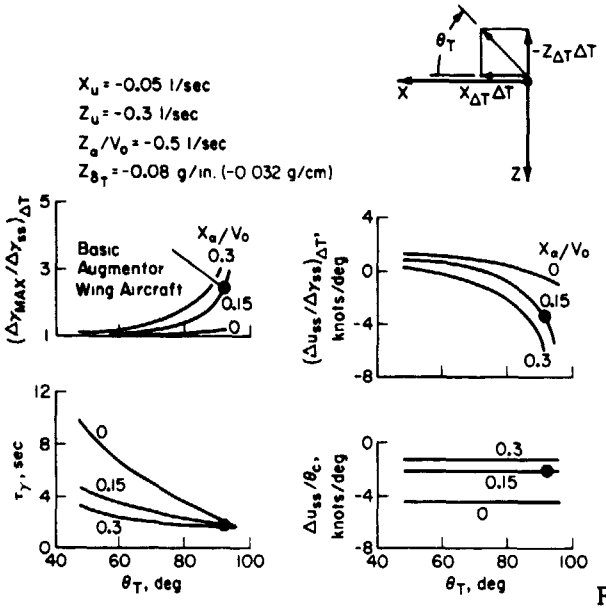

Figure 27.- Contribution of thrust inclination and drag due to lift.

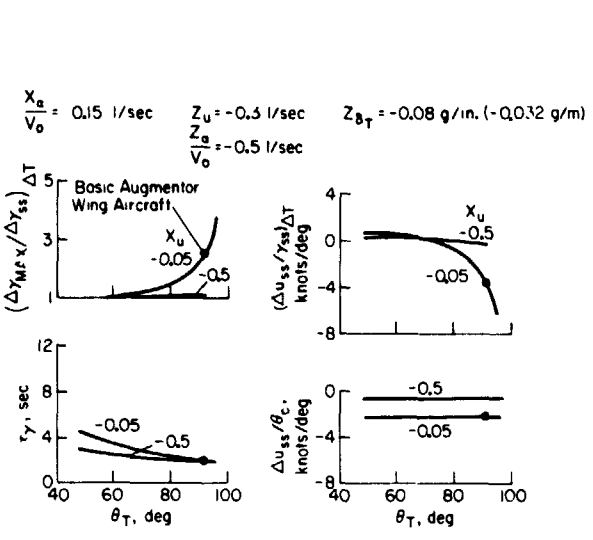

Figure 28.- Contribution of thrust inclination and axial velocity damping.

TABLE 4.- CONTRIBUTIONS TO FLIGHT-PATH AND AIRSPEED RESPONSE CHARACTERISTICS

Derivative	Response characteristics			
	τ_γ	$\left(\frac{\omega\gamma_{max}}{\Delta\gamma_{ss}}\right)_{\Delta T}$	$\left(\frac{\Delta u_{ss}}{\Delta\gamma_{ss}}\right)_{\Delta T}$	$\frac{\Delta u_{ss}}{\theta_c}$
(a) $\theta_T > 80°$				
X_α	Minimal	Large	Large	Large; independent of θ_T
X_u	Minimal	Large	Large	Moderate; independent of θ_T
(b) $45° < \theta_T < 80°$				
X_α	Large	Minimal	Moderate	Large; independent of θ_T
X_u	Moderate	Minimal	Minimal	Moderate; independent of θ_T

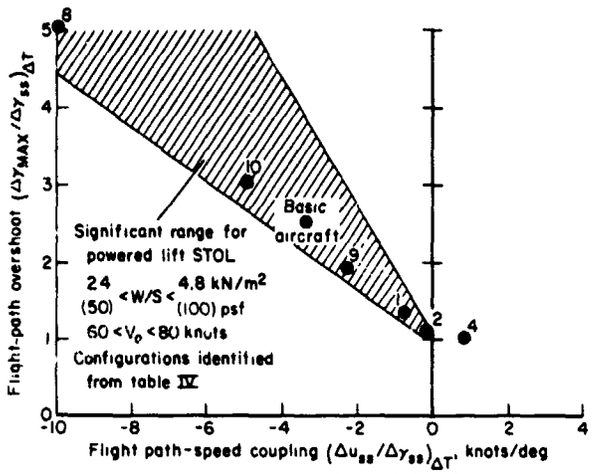

Figure 29.- Interrelationship between flight-path overshoot and flight-path/speed coupling parameters.

Sets of configurations were selected to permit independent evaluations of the path response time constant τ_γ and the speed response to attitude $\Delta u_{ss}/\theta_c$ for minimal flight-path overshoot and flight-path/speed coupling. Both the overshoot and coupling parameters were evaluated independently of the effects of initial path response to thrust (τ_γ) or of speed response to attitude ($\Delta u_{ss}/\theta_c$). As can be appreciated from the trends of the overshoot and coupling parameters in figures 27 and 28, it was not possible to evaluate them independently of each other when only X_u, X_α, or θ_T were varied. This point is also demonstrated in figure 29 by a group of experimental configurations selected from table 5 for variations in X_u, X_α, and θ_T. The correlation between path overshoot and path-speed coupling in the region $(\Delta\gamma_{max}/\Delta\gamma_{ss})_{\Delta T} > 1.3$ and $(\Delta u_{ss}/\Delta\gamma_{ss})_{\Delta T} < -1.0$ knot/deg is quite strong. Variation of either derivative Z_u or Z_α could produce independent variation in path overshoot and path-speed coupling, although neither derivative was altered in the test program. The range over which the overshoot and coupling characteristics could be considered independent due to variations in Z_u or Z_α associated with the range of wing loading and approach speed relevant to powered-lift aircraft is shown by the crosshatched region in figure 29. Evaluation of the test configurations from among those in the region indicated by

TABLE 5.- CONFIGURATIONS FOR FLIGHT-PATH AND AIRSPEED CONTROL

Configuration	X_u, 1/sec	$\frac{X_\alpha}{V_o}$, 1/sec	$\frac{X_{\Delta T}}{Z_{\Delta T}}$	ζ'_p $\left(\frac{1}{T'_{\theta_1}}\right)$, rad/sec	ω'_p $\left(\frac{1}{T'_{\theta_2}}\right)$, rad/sec	$\frac{1}{T_{\gamma_T}}$, 1/sec	$\frac{1}{T_{u_T}}$, 1/sec	τ_γ, sec	$\left(\frac{\Delta\gamma_{max}}{\Delta\gamma_{ss}}\right)_{\Delta T}$	$\left(\frac{\Delta u_{ss}}{\Delta\gamma_{ss}}\right)_{\Delta T}$, knots/deg	$\frac{\Delta u_{ss}}{\theta_c}$, knots/deg	Pilot rating	
												Pilot	
												A	B
Basic aircraft	-0.052	0.14	0.02	0.94	0.27	0.05	5.94	1.56	2.4	-3.45	-2.2	4-4-1/2	
1	-.052	.14	-.16	.94	.27	.10	-.52	1.81	1.3	-.83	-2.2	2-1/2	2-1/2
2	-.052	.14	-.3	.94	.27	.15	-.07	2.37	1.2	-.15	-2.2	2-2-1/2	
3	-.052	.14	-.56	.94	.27	.23	.17	3.16	1.05	.42	-2.2	3-1/2-4	4
4	-.052	.14	-.91	.94	.27	.34	.28	4.5	1.0	.76	-2.2	2-1/2	4
5	-.052	.3	-.62	.73	.34	.24	-.05	2.45	1.2	-.12	-1.4	2-1/2	2-1/2
6	-.052	.3	-.91	.73	.34	.33	.11	3.09	1.1	.31	-1.4	2-1/2	2-1/2
7	-.2	0.	-.32	(.26)	(.43)	.32	.39	2.89	1.0	.37	-1.5	3	4
8	-.052	.14	.11	.94	.27	.02	2.34	1.39	5.0	-10.0	-2.2	8	6-7
9	-.052	.14	-.02	.94	.27	.06	-6.37	1.57	1.9	-2.4	-2.2	3	
10	-.052	.3	-.02	.73	.34	.06	-13.7	1.49	3.0	-5.1	-1.4	4-1/2	4-1/2
11	-.052	.3	-.32	.73	.34	.15	-.51	1.89	1.5	-1.11	-1.4	3	3
12	-.052	0.	-.02	(.08)	(.44)	.06	-.71	2.02	1.1	-.26	-4.6	3-3-1/2	4-1/2
13	-.052	0.	-.32	(.08)	(.44)	.16	.39	4.42	1.0	.76	-4.6	3-3-1/2	3
14	-.052	0.	-.62	(.08)	(.44)	.25	.42	7.02	1.0	1.0	-4.6		3-1/2
15	-.2	.14	-.32	.87	.38	.32	-.04	2.36	1.1	-.04	-1.1	3	4
16	-.5	.14	-.02	.91	.54	.54	-6.37	1.85	1.0	-.28	-.6	3-1/2	2
17	-.5	.14	-.32	.91	.54	.64	-.04	2.19	1.0	-.02	-.6	3-1/2	2-1/2
18	-.5	.14	-.91	.91	.54	.88	.28	3.0	1.0	.31	-.6	3-1/2	3

solid symbols gave an appreciation of the contribution of the coupling and overshoot characteristics to handling qualities for path and speed control on the approach. Of course an independent evaluation of these two characteristics over the region of practical importance would be useful to conclusively determine if significant contributions of one characteristic exist independently of the other.

Specific test configurations for the evaluations are listed in table 5. Response parameters (that assume a step thrust input) with their corresponding transfer function factors and stability derivatives are also presented. A suitable pitch-rate command/attitude hold configuration was implemented to reduce the pilot's workload for attitude control. The characteristics of this system are indicated in figure 26.

Evaluation Task and Experimental Data

For the approach and landing, the pilot assumed control of the aircraft with it trimmed and configured for descent on the glide slope and alined with the localizer. The approach was made to a 457-m (1500-ft) STOL runway, with touchdown zone markings as indicated in figure 30. The aircraft was trimmed at 396 m (1300 ft) for descent on a 7.5° glide slope at an airspeed of 60 knots. Flaps were set at 65°, hot thrust was vectored 90° to the reference waterline of the aircraft, and power was set corresponding to 28.4 kN (6380 lb) of hot thrust. Lateral-directional stability augmentation, including roll damping, spiral mode stabilization, Dutch roll damping, and turn coordination, was used to improve the control of bank angle, heading, and sideslip so that these factors would not influence the pilot's evaluation.

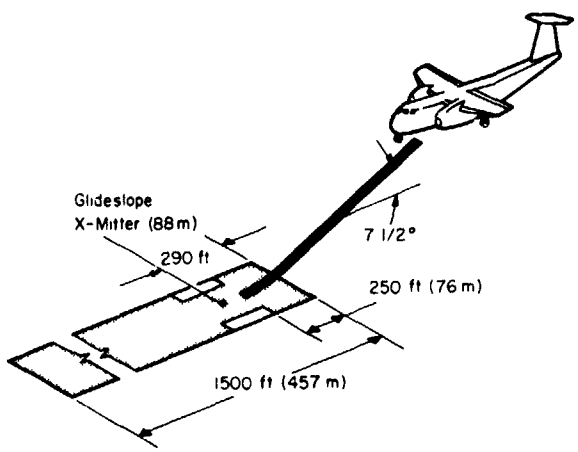

Figure 30.- STOL port configuration.

Two Ames engineering test pilots participated in the program. During the approach, the pilots introduced their own disturbances, offsets, and abuses as a means of evaluating each configuration. Both VFR and IFR evaluations were performed in calm air. Approach guidance was provided by raw ILS glide slope and localizer error information. Time histories of aircraft response and the control activity of the pilot were recorded. Pilot opinion ratings and commentary (based on the Cooper-Harper scale described in ref. 22) were obtained for each configuration concerning handling qualities associated with flight-path and airspeed control during the landing approach.

Discussion of Results

Initial flight-path response- The influence of the initial response of flight path to thrust is presented in figure 31. Pilot ratings are shown for a range of flight-path time constants (τ_γ), where the time constants are defined for a step change in thrust. The results are presented for minimal values of flight-path overshoot and flight-path speed coupling, that is, there was essentially no overshoot or coupling for these configurations. A wide range of static flight-path/velocity gradients was included in these configurations, from an extreme backside of the drag curve ($d\gamma/dV$ = 0.47 deg/knot) to an extreme front side ($d\gamma/dV$ = -1.23 deg/knot).

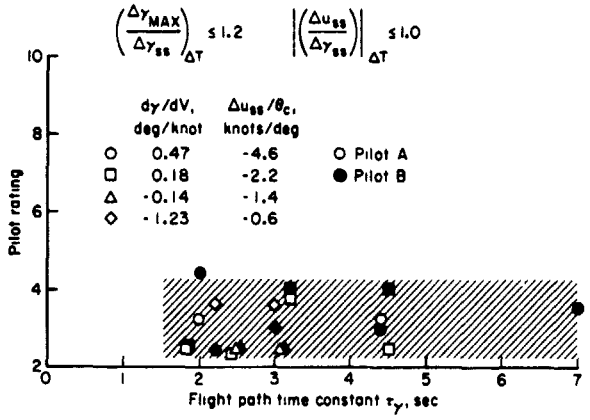

Figure 31.- Influence of initial flight-path response.

The pilot ratings appear to be insensitive to variations in τ_γ over the range of configurations tested. The results are understandable in light of the evaluation task. During the approach, extremely rapid path corrections are not required and, as the pilots indicate, any corrections can be made readily for the various configurations shown in figure 31. For these configurations, with the effects of engine acceleration and deceleration included, figures 7, 17, and 21 verify that the required path control bandwidths of 0.5 to 0.7 rad/sec can be achieved with little demand for compensation placed on the pilot.

Scatter in these pilot rating data somewhat exceed the ±1/2 rating unit variation that has come to be expected from experienced evaluation pilots. If the scatter is anything other than random in origin, it could be considered to result from a moderate influence of the range of flight path/velocity ($d\gamma/dV$) gradients included in these configurations. In fact, the pilots were somewhat dissatisfied with the extreme backside or frontside configurations ($d\gamma/dV$ = 0.47 or -1.23 deg/knot). However, their objections were based on the excessive sensitivity of speed to changes in attitude of the former and the insensitivity of speed to changes in attitude of the latter. In neither case did any consideration of the stability of closed-loop flight-path control with attitude associated with path or speed divergences influence their ratings.

Note that the configurations of the foregoing discussion were evaluated for a throttle sensitivity of Z_{δ_T} = -0.08 g/in. (-0.032 g/cm). Thus, the sensitivity of the flight-path response to a throttle input varied in direct proportion to τ_γ, that is,

$$\frac{\gamma_{ss}}{\delta_T} = \left(\frac{Z_{\delta_T}}{V_o}\right)\tau_\gamma \qquad (20)$$

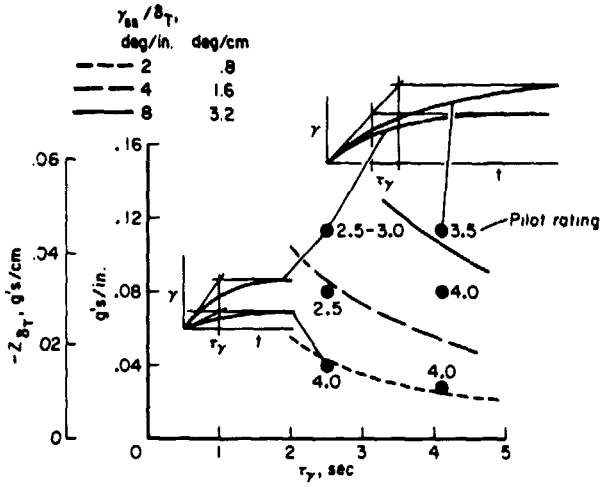

Figure 32.- Effects of throttle sensitivity on flight-path control.

A group of configurations was selected to assess the pilot's choice of throttle sensitivity Z_{δ_T} (in g/in.) compared to γ_{ss}/δ_T (in deg/in.) for τ_γ from 2.5 to 4.1 sec. Pilot ratings are shown for the test configurations in figure 32. While no strong trends in pilot rating emerge from these data, the pilot commentary indicated a preference for throttle sensitivity in terms of Z_{δ_T} in g/in. For the variation in τ_γ shown, a range of Z_{δ_T} from -0.08 to -0.1 g/in. (-0.032 to -0.039 g/cm) is most desirable. Pilot commentary revealed that flight-path response tended to be too insensitive to throttle for Z_{δ_T} below this range. For the highest Z_{δ_T}, the commentary indicated some tendency to overcorrect path with throttles, although not enough to be exceedingly objectionable. The desired range of Z_{δ_T} is somewhat lower than the optimum throttle sensitivities noted in references 8 and 23 to be approximately -0.15 g/in. (-0.058 g/cm). Sources of this disagreement conceivably lie in differences between the Augmentor Wing Aircraft simulation and the flight task, type of aircraft, and thrust control arrangement for the aircraft in references 8 and 23. These reports contain data from helicopters in flight hover tests and ground-based simulation of STOL transport aircraft. Thrust controls ranged from collective levers to conventional floor pedestal throttles. The Augmentor Wing Aircraft has two throttles located on an overhead quadrant similar to the arrangement in the original de Havilland C-8A Buffalo airframe. With this arrangement, it is more difficult to position the throttles precisely and to maintain a position reference than with a conventional floor pedestal throttle.

Flight-path/airspeed coupling- Flight-path overshoot $(\Delta\gamma_{max}/\Delta\gamma_{ss})_{\Delta T}$ and flight-path/speed coupling $(\Delta u_{ss}/\Delta\gamma_{ss})_{\Delta T}$ are two characteristics of response to thrust (as previously noted) which could not be evaluated independently in this program. They are strongly interrelated because of their mutual sensitivity to changes in longitudinal (X-axis) force characteristics (such as trimmed drag, drag due to lift, and thrust inclination). However, this interrelationship is typical of powered-lift aircraft in general (fig. 29). The evaluation of mutual changes in these two parameters conducted in this program offers insight into their influence on path and speed control for this category of aircraft. Results are presented in figure 33, with pilot ratings plotted against the path-speed coupling parameter $(\Delta u_{ss}/\Delta\gamma_{ss})_{\Delta T}$. The pilots felt that the influence of path-speed coupling was the primary contribution to their evaluation and rating and hence it was the parameter used to interpret the data.

It is apparent that path-speed coupling has a pronounced effect on pilot ratings of path-speed control. In particular, a significant degradation in ratings is noted for values of $(\Delta u_{ss}/\Delta\gamma_{ss})_{\Delta T}$ more negative than -3 knot/deg.

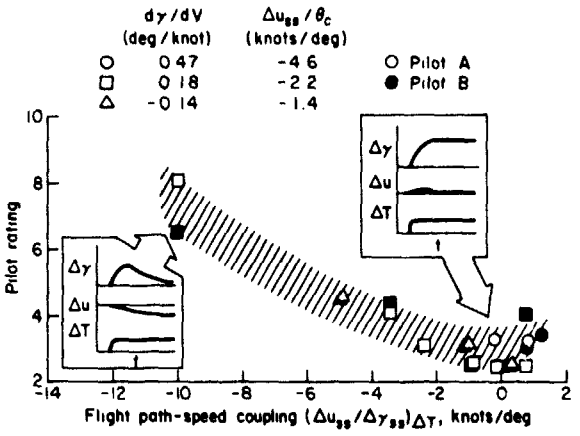

Figure 33.- Influence of flight-path/airspeed coupling.

The adverse nature of the open-loop speed response to a flight-path change with thrust is illustrated by the inset diagram at the left of the figure, where an increase in thrust to shallow the path causes the aircraft to decelerate, which, in turn, washes out the intended path correction. Such behavior is particularly undesirable since the strongly coupled response demands that the pilot pay considerable attention to path and speed control and that he work in a continuous, coordinated, closed-loop fashion with attitude and thrust to achieve adequate precision of flight-path control. Furthermore, the attitude control technique required to hold speed constant while while making a path correction with thrust is unnatural. The pilot must lower the nose to hold speed while he attempts to reduce the rate of descent and vice versa. For these two reasons, strong path-speed coupling can make the aircraft unacceptable for flying the STOL approach. In particular, for the highly coupled configuration ($\Delta u_{ss}/\Delta\gamma_{ss}$ = -10 knots/deg) corrections back to the glide slope for either high or low offsets were quite difficult to make. An example of glide-slope tracking for this configuration was shown previously in figure 1.

Airspeed-attitude sensitivity- To conclude the discussion of path and speed control for the approach, the significance of speed behavior in response to its primary control, pitch attitude, must be determined. The parameter for evaluation is the steady speed change in response to a change in pitch attitude ($\Delta u_{ss}/\theta_c$). It should be clear from the relationships associated with equation (19) that speed response to attitude and path-velocity ($d\gamma/dV$) characteristics are strongly related through their mutual dependence on the level of trimmed drag and drag due to lift. This interrelation was brought out previously in the peripheral discussion related to figure 31 and the initial flight-path response on page 32. The interrelationship provides for large speed changes with attitude for operation on the backside of the thrust-required curve and small speed changes with attitude for operation on the front side. For the control technique used in these simulation evaluations of path and speed response (speed control with attitude, path control with thrust), considerations related to speed response to attitude appear to be more important than the degree of frontside or backside operation involved.

The significance of speed control with attitude is indicated in figure 34. Pilot ratings for variations in the speed response parameter $\Delta u_{ss}/\theta_c$ are plotted for otherwise favorable values of τ_γ and $(\Delta u_{ss}/\Delta\gamma_{ss})\Delta T$. Variations in speed sensitivity to attitude have only a modest effect on pilot ratings. As expected, the pilots objected, although not too strongly, to insensitive or excessively sensitive speed response to attitude changes.

Poor harmony between speed and attitude either required objectionably large attitude changes for ordinary speed control or an unnecessarily fine touch on attitude control to avoid objectionable speed excursions. Proper harmony for speed control seems to dictate a speed-attitude sensitivity of $\Delta u_{ss}/\theta_c$ between -1.5 and -2.5 knots/deg.

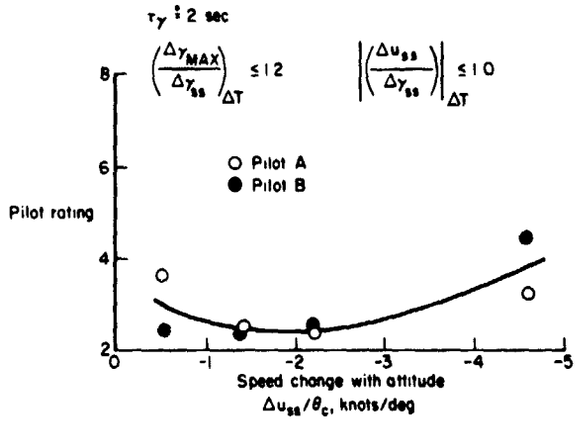

Figure 34.- Speed response to pitch attitude.

SECTION 4

COMPARISON WITH FLIGHT DATA

A limited quantity of data exists from flight tests conducted to date on powered-lift V/STOL aircraft operating on steep landing approach paths. The data concerning pilot evaluation of flight-path control and documentation of flight-path and airspeed response to thrust exist in various degree of detail. They are reviewed here to permit a qualitative comparison with the trends obtained from the current simulation results.

The aircraft considered are the NASA/DITC Augmentor Wing Research Aircraft, the Dornier DO-31, and the Breguet 941. Data are in the form of pilot commentary for flight-path control with thrust during landing approach. Where available, open-loop path and speed response to thrust for a constant attitude (or nearly so) are excerpted from flight records. In other cases, these response data are not available from flight records but can be obtained from simulations based on flight-measured performance, stability, and control characteristics. These data are summarized in table 6.

TABLE 6.- SUMMARY OF FLIGHT-PATH AND AIRSPEED RESPONSE CHARACTERISTICS OF THREE POWERED-LIFT AIRCRAFT

Aircraft (data source)		τ_γ, sec	$\left(\frac{\Delta\gamma_{max}}{\Delta\gamma_{ss}}\right)_{\Delta T}$	$\left(\frac{\Delta u_{ss}}{\Delta\gamma_{ss}}\right)_{\Delta T}$, knots/deg	$\frac{\Delta u_{ss}}{\theta_c}$, knots/deg	X_u, 1/sec	$\frac{X_\alpha}{V_o}$, 1/sec	Z_u, 1/sec	$\frac{Z_\alpha}{V_o}$, 1/sec	$\frac{X_{\Delta T}}{Z_{\Delta T}}$
Augmentor Wing Buffalo (flight) V = 65 knots δ_f = 65°	δ_ν = 75° γ = -7.5°	(a)	(a)	-2.0 to -3.3	(a)	(b)	(b)	(b)	(b)	(b)
	δ_ν = 60° γ = -6°	(a)	(a)	-0.25 to -0.75	(a)	(b)	(b)	(b)	(b)	(b)
Dornier-31 (flight) γ = -7° ν = 120° a_{x_o} = -0.05 g	Lift eng V = 70 knots	1.5	1.3	0	(a)	(b)	(b)	(b)	(b)	-0.26
	Main eng V = 85 knots	2.7	1.0	-4.0	(a)	(b)	(b)	(b)	(b)	0.58
Breguet-941 (simulator) Transparency in γ = -7.5° δ_f = 98°	60 knots	2.5	1.1	-0.45	-1.33	-0.13	0.093	-0.36	-0.49	-0.17
	65 knots	3.0	1.0	0.40	-1.7	-0.12	0.024	-0.33	-0.68	-0.17

[a] Flight data poorly suited for measuring the parameter.
[b] Data not determined from analysis of flight measurements.

NASA/DITC Augmentor Wing Research Aircraft

The aircraft has been described in some detail previously in section 3. It has been in flight status since June 1972 and is currently undergoing flight testing to document its performance, stability, and control characteristics. At this point, no stability augmentation has been provided for longitudinal control. Limited handling qualities evaluations have been conducted for the landing approach and these data are discussed here.

Approaches have been conducted on 7.5° glide slopes at speeds from 60 to 70 knots. The flap setting for these approaches was 65°, with nominal nozzle deflections of either 60° or 75°. Figure 35 shows examples of flight-path and airspeed response to thrust for these flight conditions. Although no attitude stabilization was available in the longitudinal control system, the pilot normally controlled attitude precisely during these approaches. For the 60° nozzle trim conditions, flight-path corrections were made with little associated variation in airspeed. Path-speed coupling $(\Delta u_{ss}/\Delta\gamma_{ss})_{\Delta T}$ measured in flight (table 6) ranges from -0.25 to -0.75 knots/deg. In figure 35, the path correction for the 60° nozzle angle was made with very little overshoot. Attitude is held within ±1° and a small decrease in speed, in the long-term, accompanies the increase in thrust and the positive path correction. For the 75° nozzle trim condition, more significant speed variations accompany path corrections. Path-speed coupling in this case ranges from -2.0 to -3.3 knots/deg. More overshoot is apparent in the path response and, as noted, the speed variations are more substantial than for the 60° nozzle configuration. Attitude variations are again held within ±1° of the nominal.

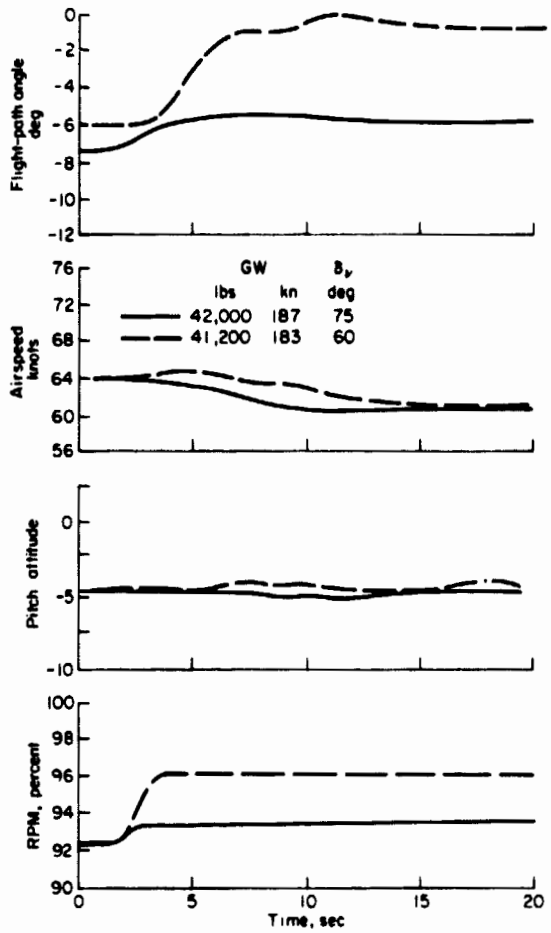

Figure 35.- Flight-path and airspeed response to thrust for Augmentor Wing Research Aircraft.

Pilot evaluations of flight-path control have been obtained to date for V/R landing approaches on a 7.5° glide slope in the 75° nozzle configuration. Visual approach guidance was provided by an optical landing aid. Thrust control of flight path has been found to provide a capability for making quite rapid flight-path corrections. However, if appreciable path corrections are attempted, large airspeed excursions occur, as would be expected from the degree of flight-path/speed coupling noted in table 6 and figure 35. The pilot objected to these speed excursions and was reluctant to attempt to control speed tightly because of the wrong sense of the attitude change associated with the flight-path correction ($\Delta\theta/\Delta\gamma$ negative). A pilot rating of 4-1/2 was given for flight-path control on the approach. Both the pilot commentary and rating support the results of the simulation as noted in figure 33. Additional objections were raised concerning the sensitivity of thrust to throttle movement and the hysteresis in the throttle-fuel control cable and linkage system. Both characteristics made it difficult for the pilot to control flight path with the throttles. However, it was indicated that reduction of the sensitivity and hysteresis would not improve flight-path control substantially due to the path-speed coupling.

Dornier DO-31

The Dornier DO-31 is a jet-lift VTOL transport aircraft powered by two main engines and eight lift engines. Figure 36 is a three-view sketch and perspective of the aircraft. The main engines of the aircraft are located at midspan of each wing and provide thrust vectoring from 10° to 120° referenced to the aircraft waterline (fig. 37). The lift engines are mounted four to a pod in each wing tip and are vectored 15° aft of the vertical. Pitch is controlled through an attitude command system that uses the elevator and pitch nozzle controls. Additional descriptive data are provided in table 7 and reference 3.

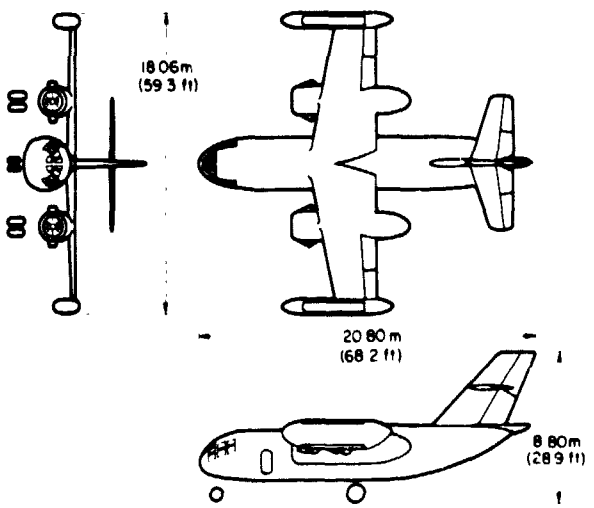

Figure 36.- Dornier DO-31 jet VTOL transport.

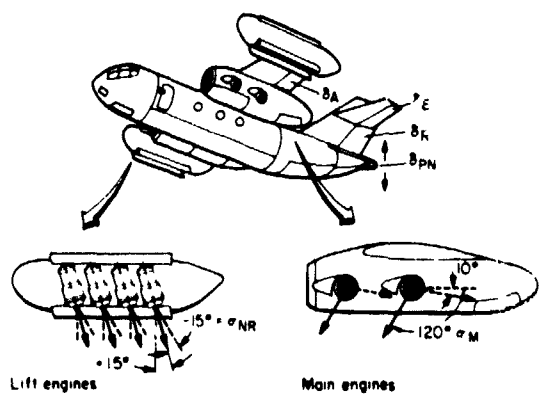

Rotation

1 Longitudinal stick, δ_{MP}, controls elevator (δ_E) and pitch nozzle (δ_{PN})

2 Lateral stick, δ_{LP}, controls ailerons (δ_A) and differential thrust of lift engines ($FCU_L - FCU_R$)

3 Rudder pedal, δ_{NP}, controls rudder (δ_R) and differential lift engine nozzle deflection ($\sigma_{NL} + \sigma_{NR}$)

Translation

1 One lift engine throttle, σ_{FCU}, controls thrust of lift engines collectively

2 Two main engine throttles, σ_{TL} and σ_{TR}, control thrust of each main engine

3 One main engine nozzle lever, σ_M, controls deflection of all main engine nozzles collectively

Figure 37.- Schematic of control functions - DO-31.

Flight operations relevant to this report were decelerating landing approaches conducted along a 7° approach path at speeds between 75 and 90 knots down to an altitude of 70 m (230 ft). Attitude was maintained constant through the attitude control system during the approach and airspeed was controlled by vectoring the main engine nozzles. Flight path could be controlled either by modulating the thrust of the lift engines or of the main engines. As indicated in table 6, path control can be achieved with the lift engines without inducing speed excursions. Figure 38 indicates an example taken from reference 3. The path correction is accomplished with little overshoot and a time constant of approximately 1.5 sec (measured after the thrust increment is attained). No speed change is apparent. A constant 5° nose-down attitude is maintained through the maneuver. In contrast, path control with the main engines (with nozzles vectored 120°) produces significant speed excursions. Table 6 indicates a path-speed coupling of -4.0 knots/deg. A time history of a path correction with the main engines is also reproduced from reference 3 in figure 38. The flight-path response is first order in nature with a time constant of 2.7 sec. A substantial speed decay accompanies the reduction in

TABLE 7.- AIRCRAFT DIMENSION AND DESIGN DATA - DORNIER DO-31

JET VTOL TRANSPORT

Wing:		
Area, m^2 (ft^2)	57.0	(613)
Span, m (ft)	17.0	(55.8)
Mean aerodynamic chord, m (ft)	3.415	(11.2)
Aspect ratio	5.05	
Sweep, deg	8.5	
Flap deflection (max), deg	45	
Aileron deflection, deg	±25	
Horizontal tail:		
Area, m^2 (ft^2)	16.4	(176)
Span, m (ft)	8.0	(26.2)
Elevator deflection, deg	±25	
Vertical tail:		
Total area, m^2 (ft^2)	15.4	(166)
Span, m (ft)	4.4	(14.4)
Rudder deflection, deg	±30	
Mass:		
Maximum conventional takeoff, kg (lb mass)	24,500	(53,900)
Maximum vertical takeoff, kg (lb mass)	21,800	(48,000)
Standard empty, kg (lb mass)	16,594	(34,300)
Weight:		
Maximum vertical takeoff, N (lb force)	213,000	(48,000)
Moment of inertia for 20,500-kg mass (45,000-lb mass) and gear down:		
I_{xx}, kg m^2 (slug-ft^2)	385,000	(284,000)
I_{yy}, kg m^2 (slug-ft^2)	277,000	(205,000)
I_{zz}, kg m^2 (slug-ft^2)	606,000	(447,000)
Center of gravity:		
Percent of mean aerodynamic chord	23.0	
Propulsion system:		
Main engine, two installed		
Rolls Royce Pegasus 5-2 turbofan		
Maximum thrust per engine at sea-level standard for 2-1/2 min, N (lb force)	67,200	(15,100)
Lift engine, eight installed		
Rolls Royce RB-162-4D lift jet		
Maximum thrust per engine at sea-level standard, N (lb force)	18,700	(4,200)
Total maximum thrust at sea-level standard, N (lb force)	285,000	(64,000)

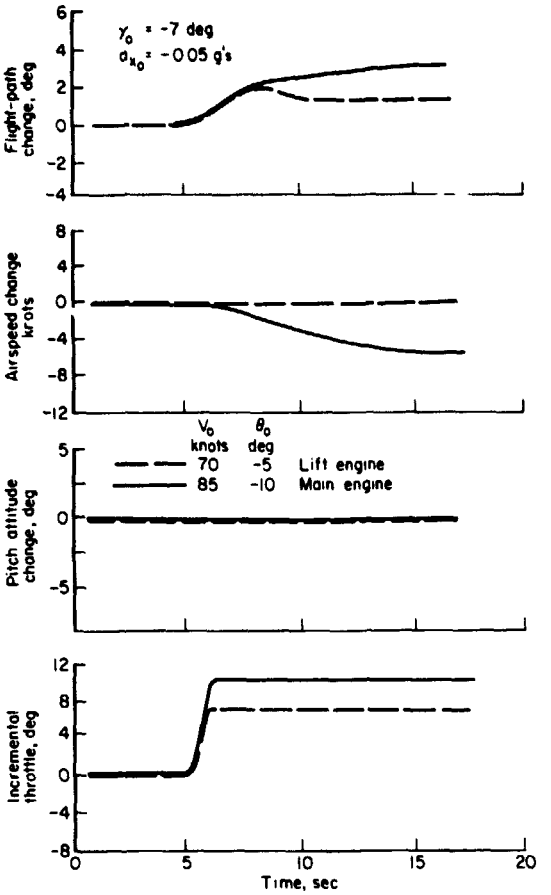

Figure 38.- Flight-path and airspeed response to a thrust change for the DO-31 during a steep, decelerating approach.

approach path angle. In this instance, a 10° nose-down attitude is maintained throughout the run. No flight-path overshoot is present since this flight condition is on the front side of the drag curve.

Pilot evaluations of flight-path control with lift engines or main engines are excerpted from reference 3. Pilots preferred to use lift engines for path control and could achieve good glide-slope tracking if corrections greater than the ±0.1 g authority of the lift engines were not required. Within this range, path control was quite precise and speed excursions were minimal. The pilots felt that path control with the main engines was unsatisfactory because of the undesirable speed perturbations that required them to modulate the nozzle control for thrust vectoring so that speed could be controlled satisfactorily. No pilot ratings were assigned for glide-slope tracking; however, the pilot commentary relative to the aircraft behavior qualitatively supports the results obtained in the current simulation.

Breguet 941

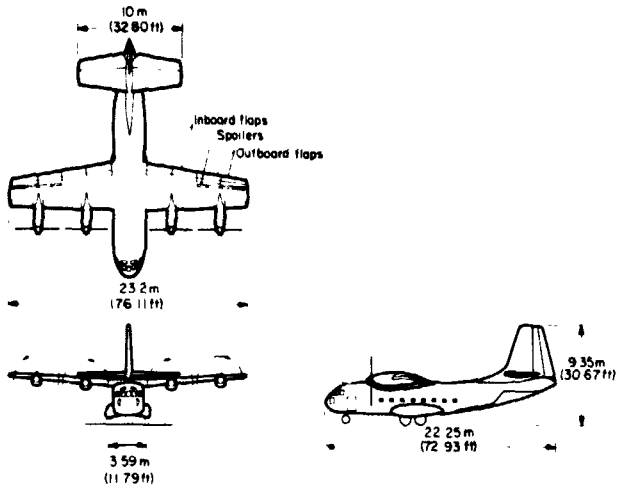

Figure 39.- Schematic of the Breguet-941.

The Breguet 941 is a high-wing, turboprop STOL transport aircraft of the deflected-propeller slipstream, mechanical flap concept (fig. 39). It is powered by four interconnected gas turbine engines. The wing is almost fully immersed in the propeller slipstream and is equipped with a large deflection (95°), full-span, triple-slotted flap. Pitch is controlled with the elevator. A propeller "transparency" mode (differential inboard-outboard pitch) is available to increase descent capability. The aircraft is described in more detail in table 8 and in references 2 and 24.

TABLE 8.- GEOMETRIC DATA FOR BREGUET-941 DEFLECTED PROPELLER SLIPSTREAM STOL TRANSPORT

Wing	
Area, m^2 (ft^2)	83 (889)
Span, m (ft)	23.2 (76.1)
Mean aerodynamic chord (reference), m (ft)	3.7 (12.15)
Incidence root, from fuselage reference line, deg	3
Aspect ratio	6.52
Flap deflection (maximum), deg	Inboard 98, outboard 72
Spoiler spanwise location	from 56 to 97 percent of span
Spoiler deflection, deg	45
Horizontal tail	
Total area, m^2 (ft^2)	30 (320)
Span, m (ft)	10 (32.8)
Elevator deflection, deg	
Maximum trailing edge up	-30
Maximum trailing edge down	+24
Stabilizer deflection, deg	+1 to +9 to fuselage ref. (leading edge up)
Vertical tail	
Total area, m^2 (ft^2)	20.3 (219)
Span, m (ft)	5.5 (17.9)
Rudder deflection, deg	
First rudder	±20
Second rudder	±40
Moment of inertia (approximate for 38,500-lb gross weight)	
I_{xx}, kg-m^2 (slug-ft^2)	305,000 (225,000)
I_{yy}, kg-m^2 (slug-ft^2)	190,000 (140,000)
I_{zz}, kg-m^2 (slug-ft^2)	540,000 (400,000)

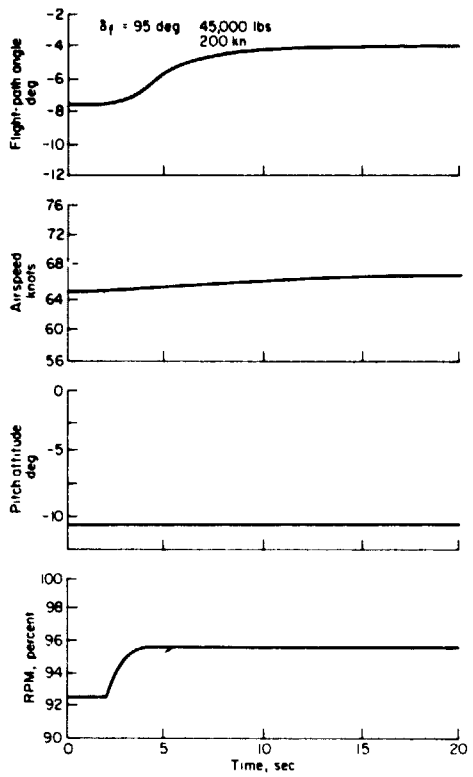

Figure 40.- Flight-path and airspeed response to thrust for the Breguet-941; 65 knots, transparency in.

Landing approaches were conducted along a 7.5° glide slope at speeds between 60 and 65 knots for the flight program reported in reference 24. Flaps were set at 98° and full transparency was used. Examples of flight-path and airspeed response to thrust at constant attitude were not available from flight data. As an alternative, these time responses were obtained from a simulation model of the aircraft based on flight-measured performance, stability, and control characteristics obtained from French and NASA flight tests conducted on the aircraft. The simulation responses are documented in reference 25 and are reproduced in figure 40 for an approach speed of 65 knots. As indicated in table 6, path response time constants were 2.5 to 3.0 sec. No overshoot is apparent in the path response. Speed excursions were minimal, with a slight increase in speed at 65 knots ($\Delta u_{ss}/\Delta\gamma_{ss}$ = 0.4 knot/deg). Commentary regarding path control (ref. 24) indicates that precise glide-slope tracking could be achieved with power. While attitude was not stabilized through the control system, a throttle interconnect prevented the inherent pitching moments due to thrust from degrading attitude control. No comments concerning speed control problems are noted. As anticipated from the current simulation results, this aircraft provides the capability for satisfactory flight-path control during the landing approach.

CONCLUSIONS

This report presents results of an analytical and experimental investigation of flight-path and airspeed control for powered-lift STOL aircraft. The study focussed on operation on the glide slope. Problems of controlling large changes in flight path or airspeed such as would be associated with transitioning from level flight onto the glide slope or flaring to a landing were not addressed.

The conclusions drawn from the simulation program are qualified where appropriate by the technique used by the pilot to control flight path and airspeed on the glide slope. With these qualifications, the following

conclusions are made from the analytical and simulation studies of flight-path and airspeed control.

- With pitch attitude stabilized, flight path controlled with thrust, and airspeed controlled with pitch attitude, the characteristics that define path and speed response as they appear to the pilot are:
  - initial flight-path time constant in response to thrust
  - overshoot in flight-path response to thrust
  - flight-path/speed coupling defined by the change in speed following a path correction with thrust
  - speed change due to a change in attitude
- These path and speed response characteristics can be defined in terms of the following configuration- and flight-condition-dependent characteristics:
  - axial and vertical velocity damping - X_u and Z_α/V_o
  - axial to vertical velocity coupling - X_α and Z_u
  - effective thrust inclination - $X_{\Delta T}/Z_{\Delta T}$
- For flight-path and airspeed control on the glide slope and over a range of configuration characteristics appropriate to powered-lift STOL,
  - flight-path/airspeed coupling and the attendant flight-path overshoot are the dominant influences on handling qualities
  - the sensitivity of speed to pitch attitude has a moderate influence on handling qualities, and
  - initial flight-path time constant has a negligible effect over the range investigated ($1.5 < \tau_\gamma < 7$ sec).

It is evident from the results of this simulation that a powered-lift STOL aircraft with the proper response characteristics can be controlled quite satisfactorily during the landing approach.

Only limited flight data pertaining to flight-path and airspeed control are available for powered-lift V/STOL aircraft. In particular, few pilot ratings are available from these flight tests to provide quantitative comparisons with the simulation. However, pilot commentary and documentation of the aircraft response qualitatively support the conclusions drawn from the simulation program, specifically that flight-path coupling with airspeed substantially influences the ability of the pilot to fly the approach precisely.

The next essential step in STOL approach and landing research should be to acquire data from a properly structured set of flight experiments to substantiate the results of the foregoing analyses and simulation. One specific objective of these flight experiments should be to independently evaluate the effects of flight-path overshoot and flight-path/airspeed coupling on glide-slope tracking.

Ames Research Center
National Aeronautics and Space Administration
Moffett Field, Calif., 94035, June 14, 1974

APPENDIX A

INFLUENCE OF PITCH ATTITUDE COMMAND AUGMENTATION ON FLIGHT-PATH AND AIRSPEED RESPONSE

This appendix describes the effects of pitch attitude stabilization on flight-path and airspeed response to commanded changes in pitch attitude or to changes in thrust. From this complete development of the response characteristics, it will be shown that the response relationships can be approximated so that the aircraft equations of motion can be simplified by ignoring the short-term attitude response and by eliminating the pitching moment equation.

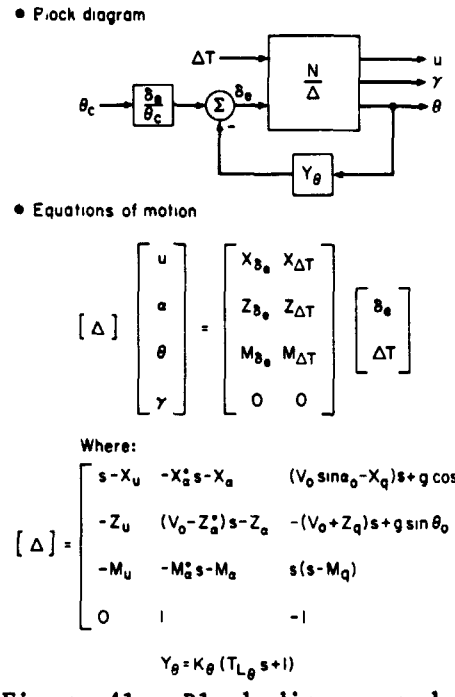

Figure 41.- Block diagram and longitudinal perturbation equations of aircraft with pitch attitude stabilization.

The relationship of attitude response to attitude command, using the matrix nomenclature for multiloop control of reference 17, follows from the longitudinal equations of motion and the control loop structure shown in figure 41:

$$\frac{\theta}{\theta_c} = \frac{(\delta_{e_c}/\theta_c)N^{\theta}_{\delta_e}}{\Delta + Y_\theta N^{\theta}_{\delta_e}} \qquad (A1)$$

The classical factors for the characteristic roots are

$$\Delta = V_o(s^2 + 2\zeta_{sp}\omega_{sp}s + \omega_{sp}^2) \times (s^2 + 2\zeta_p\omega_p s + \omega_p{}^2) \qquad (A2)$$

and, for the attitude-elevator numerator, the factors are

$$N^{\theta}_{\delta_e} = V_o(s + 1/T_{\theta_1})(s + 1/T_{\theta_2}) \qquad (A3)$$

or [2]

$$= V_o(s^2 + 2\zeta_\theta\omega_\theta s + \omega_\theta{}^2) \qquad (A4)$$

[2]Strictly speaking, the attitude numerator is approximated by $N^{\theta}_{\delta_e} = M_{\delta_e}V_o\{s^2 - [X_u + (Z_\alpha/V_o)]s + X_u(Z_\alpha/V_o) - (X_\alpha/V_o)Z_u\}$. Whether this polynomial factors into a complex pair or into two real roots depends on the magnitude of the derivatives X_α and Z_u. Large values of X_α and Z_u tend to produce the complex factors whereas, if X_α and Z_u are small, the factors occur in the more familiar form $(s + 1/T_{\theta_1})(s + 1/T_{\theta_2})$. For $X_\alpha = 0$ ($D_\alpha = g$), the factors are given by $1/T_{\theta_1} = -X_u$ and $1/T_{\theta_2} = -Z_\alpha/V_o$.

The closed-loop characteristic equation for the feedback control Y_θ (fig. 41) is

$$\Delta + Y_\theta N^\theta_{\delta_e} = V_o(s^2 + 2\zeta'_{sp}\omega'_{sp}s + \omega'^2_{sp})(s^2 + 2\zeta'_p\omega'_p s + \omega'^2_p) \quad \text{(A5)}$$

or

$$= V_o(s^2 + 2\zeta'_{sp}\omega'_{sp}s + \omega'^2_{sp})(s + 1/T'_{\theta_1})(s + 1/T'_{\theta_2}) \quad \text{(A6)}$$

depending on whether the numerator $N^\theta_{\delta_e}$ factors into two real roots or a complex pair and how tightly the attitude loop is closed. An example of the closed-loop characteristics is shown in the root-locus and Bode plot of figure 42. The compensation provided by Y_θ in the feedback loop is intended to

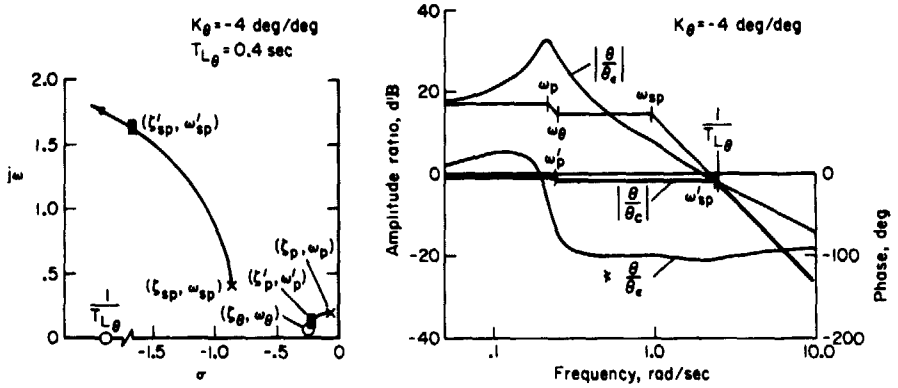

Figure 42.- Pitch attitude loop closure.

produce K/s characteristics in the crossover region for the attitude transfer function. It is apparent that both the short-period and phugoid mode damping are increased and that the bandwidth of the system is extended to higher frequencies than for the open-loop response. The phugoid roots are driven near the roots of the attitude numerator. The ratio of the frequencies of the short period and phugoid is increased from a factor of 5 to a factor of 10.

The influences of the attitude loop closure on the transfer functions for flight-path and airspeed control with attitude or thrust (section 2) are now described. The path and speed transfer functions with respect to attitude are

flight path:

$$\left(\frac{\gamma}{\theta_c}\right)_{\theta\to\delta_e} = \frac{N^\gamma_{\theta_c}}{\Delta + Y_\theta N^\theta_{\delta_e}} \quad \text{(A7a)}$$

airspeed:

$$\left(\frac{u}{\theta_c}\right)_{\theta\to\delta_e} = \frac{N^u_{\theta_c}}{\Delta + Y_\theta N^\theta_{\delta_e}} \quad \text{(A7b)}$$

The numerators for these two transfer functions are identical to the elevator control numerators $N^\gamma_{\delta_e}$ and $N^u_{\delta_e}$ and are unmodified by the attitude loop closure. They are, respectively,

$$N^\gamma_{\theta_c} = A_{\gamma_\theta}(\delta_e/\theta_c)(s + 1/T_{\gamma_1})(s + 1/T_{\gamma_2})(s + 1/T_{\gamma_3}) \quad \text{(A8)}$$

and

$$N^u_{\theta_c} = A_{u_\theta}(\delta_e/\theta_c)(s + 1/T_{u_1})(s + 1/T_{u_2})(s + 1/T_{u_3}) \quad \text{(A9)}$$

The complete path and speed transfer functions to an attitude command are written:

$$\left(\frac{\gamma}{\theta_c}\right)_{\theta\to\delta_e} = A_{\gamma_\theta} \frac{(\delta_e/\theta_c)(s + T_{\gamma_1})(s + 1/T_{\gamma_2})(s + 1/T_{\gamma_3})}{(s^2 + 2\zeta'_p\omega'_p s + \omega'^2_p)(s^2 + 2\zeta'_{sp}\omega'_{sp} s + \omega'^2_{sp})} \quad \text{(A10)}$$

$$\left(\frac{u}{\theta_c}\right)_{\theta\to\delta_e} = A_{u_\theta} \frac{(\delta_e/\theta_c)(s + 1/T_{u_1})(s + 1/T_{u_2})(s + 1/T_{u_3})}{(s^2 + 2\zeta'_p\omega'_p s + \omega'^2_p)(s^2 + 2\zeta'_{sp}\omega'_{sp} s + \omega'^2_{sp})} \quad \text{(A11)}$$

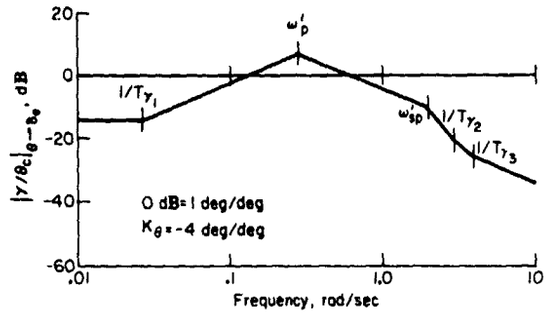

Figure 43.- Flight-path response to pitch attitude with pitch attitude stabilized.

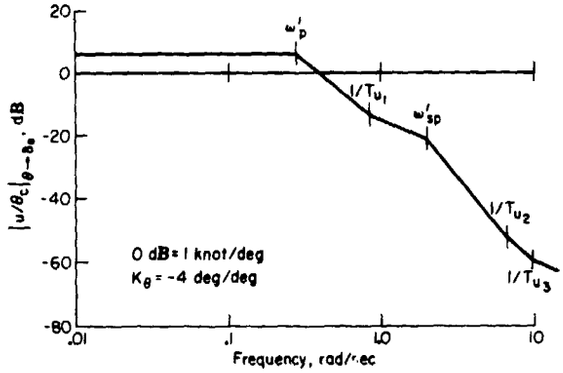

Figure 44.- Airspeed response to pitch attitude with pitch attitude stabilized.

Typical examples of these two transfer functions are seen in the Bode plots of figures 43 and 44. From these Bode plots and from equations (A10) and (A11), it is apparent that path and speed response to attitude are dominated by the closed-loop phugoid mode and the low-frequency numerator roots $1/T_{\gamma_1}$ and $1/T_{u_1}$. The magnitude of response at the short period is of little consequence when compared to the phugoid response. Furthermore, the roots at $1/T_{\gamma_2}$ and $1/T_{\gamma_3}$ or at $1/T_{u_2}$ and $1/T_{u_3}$ are typically at higher frequency than the closed-loop short period and may be ignored. In fact, these transfer functions can be approximated by neglecting the high-frequency factors and replacing the phugoid roots with their near equivalent, the factors of the attitude numerator, that is,

$$\left.\begin{aligned} \left(\frac{\gamma}{\theta_c}\right)_{\theta\to\delta_e} &= \frac{A_{\gamma_\theta}(s + 1/T_{\gamma_1})}{s^2 + 2\zeta_\theta\omega_\theta s + \omega_\theta{}^2} \\ \left(\frac{u}{\theta_c}\right)_{\theta\to\delta_e} &= \frac{A_{u_\theta}(s + 1/T_{u_1})}{s^2 + 2\zeta_\theta\omega_\theta s + \omega_\theta{}^2} \end{aligned}\right\} \quad \text{(A12)}$$

Figures 45 and 46 compare these approximations with the actual path and speed transfer functions. The path and speed transfer functions with respect to thrust are

flight path:

$$\left(\frac{\gamma}{\Delta T}\right)_{\theta\to\delta_e} = \frac{N^\gamma_{\Delta T} + Y_\theta N^\theta_{\delta_e} N^\gamma_{\Delta T}}{\Delta + Y_\theta N^\theta_{\delta_e}} \quad \text{(A13a)}$$

airspeed:

$$\left(\frac{u}{\Delta T}\right)_{\theta\to\delta_e} = \frac{N^u_{\Delta T} + Y_\theta N^u_{\Delta T} N^\theta_{\delta_e}}{\Delta + Y_\theta N^\theta_{\delta_e}} \quad \text{(A13b)}$$

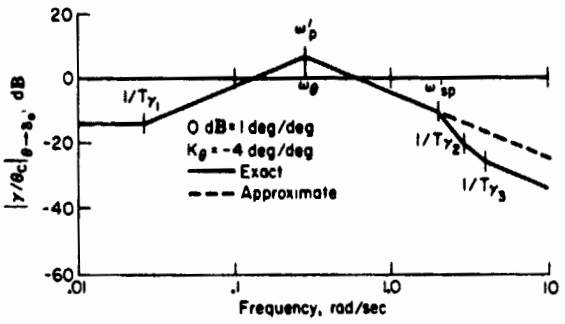

Figure 45.- Comparison of exact and approximate flight-path response to pitch attitude with pitch attitude stabilized.

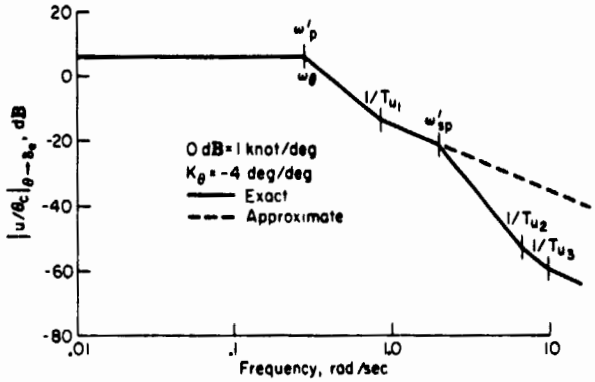

Figure 46.- Comparison of exact and approximate airspeed response to pitch attitude with pitch attitude stabilized.

It is apparent that the attitude loop closure modifies the basic path and speed numerators with respect to thrust $N^{\gamma}_{\Delta T}$ and $N^{u}_{\Delta T}$. For the flight-path response,

$$N^{\gamma}_{\Delta T} = A_{\gamma_T}(s + 1/T_{\gamma_{T_1}})(s + 1/T_{\gamma_{T_2}})$$

$$\times (s + 1/T_{\gamma_{T_3}})$$

$$= A_{\gamma_T}(s + 1/T_{\gamma_{T_1}})$$

$$\times (s^2 + 2\zeta_{\gamma_T}\omega_{\gamma_T}s + \omega^2_{\gamma_T}) \quad \text{(A14)}$$

and

$$N^{\theta}_{\delta_e}{}^{\gamma}_{\Delta T} = A_{\theta_\gamma}(s + 1/T_{\gamma_T}) \quad \text{(A15)}$$

The effect of the attitude loop closure on the roots of the numerator

$$N^{\gamma}_{\Delta T_{\theta \to \delta_e}} = N^{\gamma}_{\Delta T} + Y_\theta N^{\theta}_{\delta_e}{}^{\gamma}_{\Delta T}$$

is indicated in figure 47. In accordance with the complex polynomial factorization techniques of reference 26, the sigma Bode locus $|G(-\sigma)|$ graphically illustrates the progression of these roots from the factors of $N^{\gamma}_{\Delta T}$ for $K_\theta = 0$ to

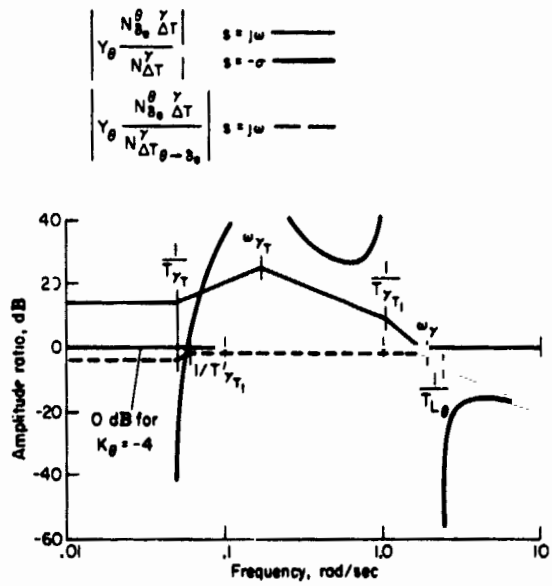

Figure 47.- Influence of pitch attitude stabilization on the roots of the numerator of the flight-path to thrust transfer function.

$N^{\gamma}_{\Delta T_{\theta \to \delta_e}}$ for values of K_θ appropriate to the attitude loop closure of figure 42. One of the roots is essentially equivalent to the factor $1/T_{\gamma_T}$ of the coupling numerator $N^{\theta}_{\delta_e}{}^{\gamma}_{\Delta T}$. The resulting transfer function for path control with thrust is

$$\left(\frac{\gamma}{\Delta T}\right)_{\theta \to \delta_e} = \frac{A'_{\gamma_T}(s + 1/T'_{\gamma T_1})(s^2 + 2\zeta_\gamma \omega_\gamma s + \omega_\gamma{}^2)}{(s^2 + 2\zeta'_p \omega'_p s + \omega'^2_p)(s^2 + 2\zeta'_{sp} \omega'_{sp} s + \omega'^2_{sp})} \tag{A16}$$

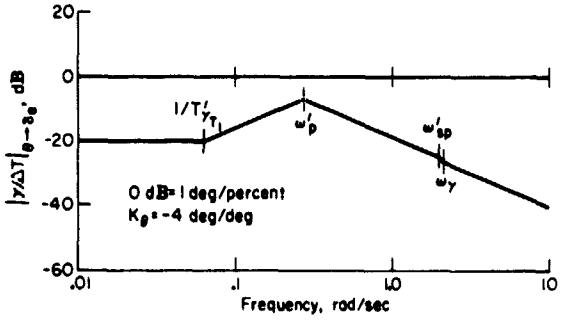

Figure 48.- Flight-path response to thrust with pitch attitude stabilized.

The Bode plot in figure 48 is an example of this transfer function. It is apparent that the dominant contributions are made by the closed-loop phugoid mode and the numerator root at $1/T_{\gamma_T}$. The remaining factors occur at high frequency and at such low magnitudes that they are of little consequence to the response.

For the airspeed response,

$$N^{u}_{\Delta T} = A_{u_T}(s + 1/T_{u_{T_1}})(s + 1/T_{u_{T_2}}) \times (s + 1/T_{u_{T_3}}) \tag{A17}$$

and

$$N^{u}_{\Delta T}{}^{\theta}_{\delta_e} = A_{u_\theta}(s + 1/T_{u_T}) \tag{A18}$$

Typical roots of the numerator

$$N^{u}_{\Delta T_{\theta \to \delta_e}} = N^{u}_{\Delta T} + Y_\theta N^{u}_{\Delta T}{}^{\theta}_{\delta_e}$$

are shown in figure 49 using the sigma Bode locus to illustrate the effect of the attitude loop closure. The roots are driven quite close to the numerator factors $N^{u}_{\Delta T}{}^{\theta}_{\delta_e}$ and Y_θ. The resulting transfer function for speed control with thrust is

$$\left(\frac{u}{\Delta T}\right)_{\theta \to \delta_e} = \frac{A'_{u_T}(s + 1/T'_{u_{T_1}})(s^2 + 2\zeta'_u \omega'_u s + \omega'^2_u)}{(s^2 + 2\zeta'_p \omega'_p s + \omega'^2_p)(s^2 + 2\zeta'_{sp} \omega'_{sp} s + \omega'^2_{sp})} \tag{A19}$$

and an example is shown in figure 50. Low-frequency modes dominate speed response, and contributions at the short-period frequency are so small that they can be ignored.

From the nature of the transfer functions for path and speed (figs. 48 and 50), it is reasonable to approximate these relationships by neglecting the higher frequency contributions and adopting a format comparable to that

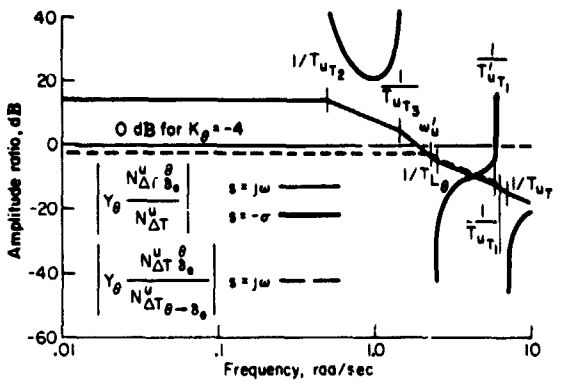

Figure 49.- Influence of pitch attitude stabilization on the roots of the numerator of the airspeed to thrust transfer function.

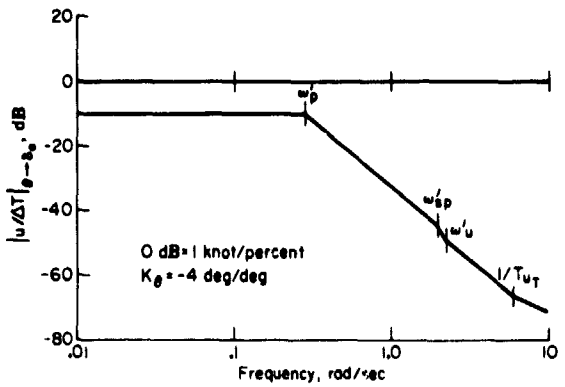

Figure 50.- Airspeed response to thrust with pitch attitude stabilized.

used in equation (A12), that is,

$$\left(\frac{\gamma}{\Delta T}\right)_{\theta \to \delta_e} = \frac{A_{\gamma_T}(s + 1/T_{\gamma_T})}{s^2 + 2\zeta_\theta \omega_\theta s + \omega_\theta{}^2} \tag{A20a}$$

and

$$\left(\frac{u}{\Delta T}\right)_{\theta \to \delta_e} = \frac{A_{u_T}(s + 1/T_{u_T})}{s^2 + 2\zeta_\theta \omega_\theta s + \omega_\theta{}^2} \tag{A20b}$$

Figures 51 and 52 compare these approximations with the actual transfer functions.

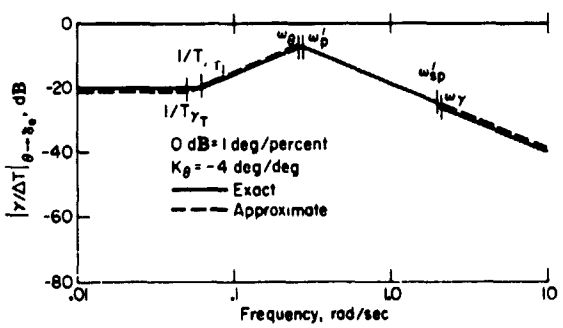

Figure 51.- Comparison of exact and approximate flight-path response to thrust with pitch attitude stabilized.

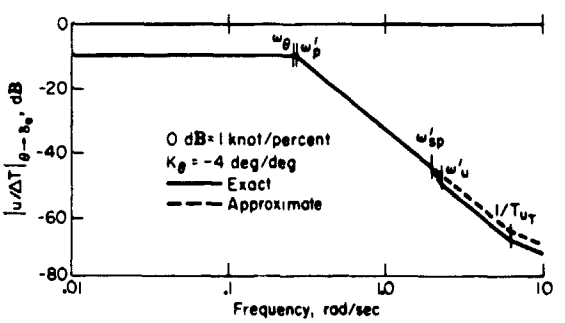

Figure 52.- Comparison of exact and approximate airspeed response to thrust with pitch attitude stabilized.

The implication of the approximations to the path and speed transfer functions (eqs. (A12) and (A20)) is that the attitude stabilization loop is closed at a sufficiently high gain so that $\theta = \theta_c$ over the frequency range of interest. In fact, for infinite attitude gain ($K_\theta = \infty$), these approximations become exact, with the result that the equations of motion for the

aircraft with infinitely tight attitude stabilization can be simplified to

$$\begin{bmatrix} s - X_u & -X_\alpha & 0 \\ -Z_u & V_o s - Z_\alpha & 0 \\ 0 & 1 & 1 \end{bmatrix} \begin{Bmatrix} u \\ \alpha \\ \gamma \end{Bmatrix} = \begin{bmatrix} -g \cos \theta_o & X_{\Delta T} \\ V_o s - g \sin \theta_o & Z_{\Delta T} \\ 1 & 0 \end{bmatrix} \begin{Bmatrix} \theta_c \\ \Delta T \end{Bmatrix} \qquad \text{(A21)}$$

APPENDIX B

NOTATION

A_{u_T}	gain of the thrust to speed transfer function, ft/sec/lb, m/sec/kN
$A_{u\gamma}$	gain of the $N^{u}_{\theta_c}\,^{\gamma}_{\Delta T}$ coupling numerator
A_{u_θ}	gain of the attitude to speed transfer function, ft/sec/rad, m/sec/rad
A_{γ_T}	gain of the thrust to flight-path transfer function, rad/lb, rad/kN
A_{γ_θ}	gain of the attitude to flight-path transfer function, rad/rad
a_x	longitudinal acceleration, g
a_z	normal acceleration, g
C_D	drag coefficient
C_{D_α}	dimensionless derivative of drag due to angle of attack, $\frac{1}{\bar{q}S_W}\frac{\partial D}{\partial \alpha}$
C_j	thrust coefficient for cold blowing air, $\frac{T_{cold}}{\bar{q}S_W}$
C_L	lift coefficient
C_{L_α}	dimensionless lift-curve slope, $\frac{1}{\bar{q}S_W}\frac{\partial L}{\partial \alpha}$
$\bar{c}$	mean aerodynamic chord MAC
D	total drag, $C_D\bar{q}S_W$
DITC	Canadian Department of Industry, Trade, and Commerce
D_α	drag derivative due to angle of attack, $\frac{1}{m}\frac{\partial D}{\partial \alpha}$; ft/sec^2/rad, m/sec^2/rad
$\frac{d\gamma}{dV}$	change of flight path with airspeed for constant thrust, deg/knot
e	exponential function
F_c	control column force, lb, kN
GW,W	gross weight, lb, kN
g	acceleration due to gravity, ft/sec^2, m/sec^2
H_e	elevator hinge moment, ft-lb, kN-m
H_{δ_e}	dimensional elevator hinge moment derivative due to elevator deflection, $\frac{1}{I_e}\frac{\partial H_e}{\partial \delta_e}$, rad/sec^2/rad

$H_{\dot{\delta}_e}$	dimensional elevator hinge moment derivative due to elevator deflection rate, $\frac{1}{I_e}\frac{\partial H_e}{\partial \dot{\delta}_e}$, 1/sec
h	altitude, ft, m
$\dot{h}$	vertical velocity, ft/sec or ft/min, m/sec
I_e	elevator moment of inertia, slug-ft^2, kg-m^2
I_x	roll moment of inertia, slug-ft^2, kg-m^2
I_y	pitch moment of inertia, slug-ft^2, kg-m^2
I_z	yaw moment of inertia, slug-ft^2, kg-m^2
I_{xz}	cross-product of inertia, slug-ft^2, kg-m^2
IFR	instrument flight rules
ILS	instrument landing system
j	complex number $(-1)^{1/2}$
K_I	gain for pitch rate command integrator, deg/sec/in., deg/sec/cm
K_q	pitch rate feedback gain to elevator, deg/deg/sec
K_u	airspeed feedback gain to nozzle, deg/knot; pilot airspeed-attitude gain
K_α	angle-of-attack feedback gain to nozzle, deg/deg
K_δ	column position feedforward gain, deg/in., deg/cm
K_γ	pilot flight-path - throttle gain, percent/deg
K_θ	pitch attitude feedback gain to elevator, deg/deg
M	pitching moment, ft-lb, kN-m
M_q	pitch-rate damping, $\frac{1}{I_y}\frac{\partial M}{\partial q}$, 1/sec
M_u	pitch acceleration derivative due to forward speed, $\frac{1}{I_y}\frac{\partial M}{\partial u}$, rad/sec^2 per ft/sec, rad/sec^2 per m/sec
M_α	longitudinal static angle-of-attack stability, $\frac{1}{I_y}\frac{\partial M}{\partial \alpha}$, rad/sec^2/ra·
$M_{\dot{\alpha}}$	pitch acceleration derivative due to rate of change of angle of attack, $\frac{1}{I_y}\frac{\partial M}{\partial \dot{\alpha}}$, 1/sec

M_{δ_e}	elevator control effectiveness, $\frac{1}{I_y}\frac{\partial M}{\partial \delta_e}$, rad/sec^2/rad
M_{δ_ν}	pitch acceleration derivative due to nozzle deflection, $\frac{1}{I_y}\frac{\partial M}{\partial \delta_\nu}$, rad/sec^2/rad
$M_{\Delta T}$	pitch acceleration derivative due to thrust, $\frac{1}{I_y}\frac{\partial M}{\partial \Delta T}$, rad/sec^2/lb, rad/sec^2/kN
m	aircraft mass, slug, kg
N_i^r	numerator of the transfer function that relates response r to an input i
$N_{\delta_e\ \Delta T}^{\theta\ \gamma}$	coupling numerator for flight-path response to thrust with attitude to elevator loop closed
$N_{\Delta T\ \delta_e}^{u\ \theta}$	coupling numerator for airspeed response to thrust with attitude to elevator loop closed
$N_{\theta_c\ \Delta T}^{u\ \gamma}$	coupling numerator for flight-path response to thrust with speed to attitude command loop closed
q, q_B	body axis pitch rate, deg/sec
$\bar{q}$	dynamic pressure, lb/ft^2, kN/m^2
S, S_W	wing area, ft^2, m^2
s	Laplace operator, $\sigma \pm j\omega$
T_{hot}	thrust component due to hot jet exhaust, lb, kN
T_{cold}	thrust of cold blowing air from augmentor flap, lb, kN
T_{L_γ}	lead time constant of the pilot transfer function for thrust control, sec
T_{L_θ}	lead time constant for $\theta \rightarrow \delta_e$ loop
t	time, sec
$\frac{1}{T_{sp_1}}, \frac{1}{T_{sp_2}}$	real roots of the longitudinal characteristic equation normally associated with the short period mode
$\frac{1}{T_{u_{T_1}}}, \frac{1}{T_{u_{T_2}}}, \frac{1}{T_{u_{T_3}}}$	real roots of the numerator of the thrust-to-airspeed transfer function
$\frac{1}{T_{u_T}}$	low-frequency root of the numerator of the thrust-to-airspeed transfer function with the attitude to elevator loop closed

$\frac{1}{T_{u_1}}, \frac{1}{T_{u_2}}, \frac{1}{T_{u_3}}$	real roots of the numerator of the attitude to airspeed transfer function
$\frac{1}{T'_{u_1}}$	real root of the characteristic equation with attitude and airspeed to elevator loops closed (rate command system)
$\frac{1}{T_{\gamma T}}$	low-frequency root of the numerator of the thrust to flight-path transfer function with the attitude to elevator loop closed
$\frac{1}{T'_{\gamma T}}$	low-frequency root of the numerator of the thrust to flight-path transfer function with the attitude and airspeed to elevator loops closed
$\frac{1}{T_{\gamma_{T_1}}}, \frac{1}{T_{\gamma_{T_2}}}, \frac{1}{T_{\gamma_{T_3}}}$	real roots of the numerator of the thrust to flight-path transfer function
$\frac{1}{T_{\gamma_1}}$	low-frequency root of the numerator of the attitude to flight-path transfer function (frequently identified in the literature as $\frac{1}{T_{h_1}}$, the low-frequency numerator factor of the elevator-to-altitude transfer function)
$\frac{1}{T_{\gamma_2}}, \frac{1}{T_{\gamma_3}}$	high-frequency real roots of the numerator of the attitude to flight-path transfer function
T_δ	pitch rate command system time constant
$\frac{1}{T_{\theta_1}}, \frac{1}{T_{\theta_2}}$	real roots of the numerator of the elevator to attitude transfer function
$\frac{1}{T'_{\theta_1}}, \frac{1}{T'_{\theta_2}}$	low-frequency real roots of the longitudinal characteristic equation (with the $\theta \rightarrow \delta_e$ loop closed) normally associated with the phugoid mode
u	perturbation airspeed, knots or ft/sec, m/sec
$u \rightarrow \theta_c$	airspeed to attitude command loop closure
u_c	commanded airspeed perturbation, knots or ft/sec, m/sec
u_ε	airspeed error, knots or ft/sec, m/sec
V_o	true airspeed, knots or ft/sec, m/sec
VFR	visual flight rules

X	longitudinal force, lb, kN
X_q	longitudinal acceleration derivative due to pitch rate, $\frac{1}{m}\frac{\partial X}{\partial q}$, ft/sec, m/sec
X_u	longitudinal acceleration derivative due to forward speed, $\frac{1}{m}\frac{\partial X}{\partial u}$, 1/sec
X_α	longitudinal acceleration derivative due to angle of attack, $\frac{1}{m}\frac{\partial X}{\partial \alpha}$ ft/sec^2/rad, m/sec^2/rad
$X_{\dot{\alpha}}$	longitudinal acceleration derivative due to angle-of-attack rate, $\frac{1}{m}\frac{\partial X}{\partial \dot{\alpha}}$, ft/sec, m/sec
X_{δ_e}	elevator drag derivative, $\frac{1}{m}\frac{\partial X}{\partial \delta_e}$, ft/sec^2/rad, m/sec^2/rad
$X_{\Delta T}$	longitudinal acceleration derivative due to thrust, $\frac{1}{m}\frac{\partial X}{\partial \Delta T}$, ft/sec^2/lb, m/sec^2/kN
X_{δ_ν}	longitudinal acceleration derivative due to nozzle deflection, $\frac{1}{m}\frac{\partial X}{\partial \delta_\nu}$, ft/sec^2/rad, m/sec^2/rad
x_{cg}	center-of-gravity location, percent mean aerodynamic chord
Y_E	transfer function for engine dynamic response
Y_{Pu}	pilot transfer function for speed control with attitude
$Y_{P\gamma}$	pilot transfer function for flight-path control with thrust
Y_{θ_c}	pilot transfer function for attitude control with elevator
Z	vertical force, lb, kN
Z_q	vertical acceleration derivative due to pitch rate, $\frac{1}{m}\frac{\partial Z}{\partial q}$, ft/sec, m/sec
Z_u	vertical acceleration derivative due to forward speed, $\frac{1}{m}\frac{\partial Z}{\partial u}$, 1/sec
Z_α	vertical acceleration derivative due to angle of attack, $\frac{1}{m}\frac{\partial Z}{\partial \alpha}$, ft/sec^2/rad, m/sec^2/rad
$Z_{\dot{\alpha}}$	vertical acceleration derivative due to angle-of-attack rate, $\frac{1}{m}\frac{\partial Z}{\partial \dot{\alpha}}$, ft/sec, m/sec
Z_{δ_e}	elevator lift derivative, $\frac{1}{m}\frac{\partial Z}{\partial \delta_e}$, ft/sec^2/rad, m/sec^2/rad

$Z_{\Delta T}$	vertical acceleration derivative due to thrust, $\frac{1}{m}\frac{\partial Z}{\partial \Delta T}$, ft/sec^2/lb, m/sec^2/kN
Z_{δ_ν}	vertical acceleration derivative due to nozzle deflection, $\frac{1}{m}\frac{\partial Z}{\partial \delta_\nu}$, ft/sec^2/rad, m/sec^2/rad
α	angle of attack, deg or rad
γ	flight-path angle, deg or rad
$\gamma \rightarrow \delta_T$	flight-path to throttle loop closure
γ_c	commanded flight-path angle, deg or rad
γ_{ss}	steady-state flight-path angle, deg or rad
γ_ϵ	flight-path angle error, deg or rad
Δ	characteristic matrix for longitudinal equations of motion; incremental value
$\left(\frac{\Delta u_{ss}}{\Delta \gamma_{ss}}\right)_{\Delta T}$	ratio of change of steady-state airspeed to flight-path due to a change in thrust (constant pitch attitude), knots/deg
$\frac{\Delta u_{ss}}{\theta_c}$	change in steady-state airspeed per unit change in pitch attitude (constant thrust), knots/deg
$\Delta\gamma_{max}$	maximum flight-path change following a change in thrust, deg
$\left(\frac{\Delta\gamma_{max}}{\Delta\gamma_{ss}}\right)_{\Delta T}$	ratio of maximum to steady-state change of flight path due to a change in thrust (constant pitch attitude)
δ_c	control column deflection, in., cm
δ_e	elevator deflection, deg
δ_{e_c}	commanded elevator deflection, deg
δ_f	flap deflection, deg
δ_T	throttle deflection, in., cm
δ_ν	nozzle deflection, deg
ζ_E, ω_E	damping ratio and natural frequency of engine thrust transfer function
ζ_p', ω_p'	damping ratio and natural frequency of the phugoid mode
$\zeta_p{}', \omega_p{}'$	damping ratio and natural frequency of the phugoid mode (with $\theta \rightarrow \delta_e$ loop closed)

ζ_{sp}, ω_{sp}	damping ratio and natural frequency of the short-period mode
$\zeta'_{sp}, \omega'_{sp}$	damping ratio and natural frequency of the short-period mode with $\theta \rightarrow \delta_e$ loop closed
ζ'_u, ω'_u	damping ratio and natural frequency of the numerator roots of the thrust to airspeed transfer function with $\theta \rightarrow \delta_e$ loop closed
$\zeta_\gamma, \omega_\gamma$	damping ratio and natural frequency of the numerator roots of the thrust to flight-path transfer function with $\theta \rightarrow \delta_e$ loop closed
$\zeta'_\gamma, \omega'_\gamma$	damping ratio and natural frequency of the numerator roots of the flight-path to thrust transfer function with the attitude and airspeed to elevator loops closed (rate command system)
$\zeta_{\gamma_T}, \omega_{\gamma_T}$	damping ratio and natural frequency of the numerator roots of the thrust to flight-path transfer function
$\zeta_\theta, \omega_\theta$	damping ratio and natural frequency of the numerator roots of the elevator to attitude transfer function
$\zeta'_\theta, \omega'_\theta$	damping ratio and natural frequency of the low-frequency characteristic roots with attitude and airspeed to elevator loops closed
θ	pitch attitude, deg
$\theta \rightarrow \delta_e$	pitch attitude to elevator loop closure
θ_c	commanded pitch attitude, deg
θ_ε	pitch attitude error, deg
θ_T	effective thrust inclination, deg
σ	real part of a complex root
τ_γ	time constant for initial flight-path response to thrust, sec
τ_e	equivalent pilot transport delay, sec
ω	frequency, rad/sec
ω_{co}	gain crossover frequency
$\dot{(\ )}$	derivative with respect to time, $\frac{d(\ )}{dt}$
$\angle(\ )$	phase angle of ( )

REFERENCES

1. Franklin, James A.; and Innis, Robert C.: Flight-Path and Airspeed Control for the STOL Approach and Landing. NASA SP-320, 1972, pp. 181-198.

2. Quigley, Hervey C.; Innis, Robert C.; and Holzhauser, Curt A.: A Flight Investigation of the Performance, Handling Qualities, and Operational Characteristics of a Deflected Slipstream STOL Transport Airplane Having Four Interconnected Propellers. NASA TN D-2231, 1964.

3. Holzhauser, Curt A.; Morello, Samuel A.; Innis, Robert C.; and Patton, James M., Jr.: A Flight Evaluation of a VTOL Jet Transport Under Visual and Simulated Instrument Conditions. NASA TN D-6754, 1972.

4. Innis, Robert C.; Holzhauser, Curt A.; and Quigley, Hervey C.: Airworthiness Considerations for STOL Aircraft. NASA TN D-5594, 1970.

5. Franklin, J. A.; and Innis, R. C.: Longitudinal Handling Qualities During Approach and Landing of a Powered Lift STOL Aircraft. NASA TM X-62,144, 1972.

6. Grantham, William D.; Nguyen, Luat T.; Patton, James M., Jr.; Deal, Perry L.; Champine, Robert A.; and Carter, C. R.: Fixed-Base Simulator Study of an Externally Blown Flap STOL Transport Airplane During Approach and Landing. NASA TN D-6898, 1972.

7. Hassell, James L.; and Judd, Joseph H.: Study of Ground Proximity Effects on Powered-Lift STOL Landing Performance. NASA SP-320, 1972, pp. 199-213.

8. Craig, S. J.; Ashkenas, I. L.; and Heffley, R. K.: Pilot Background and Vehicle Parameters Governing Control Technique in STOL Approach Situations. Rep. FAA-RD-72-69, Federal Aviation Administration, June 1972.

9. Allison, R. L.; Mack, M.; and Rumsey, P. C.: Design Evaluation Criteria for Commerical STOL Transports. NASA CR-114454, 1972.

10. Chalk, C. R.; Key, D. L.; Kroll, J.; Wasserman, R.; and Radford, R. C.: Background Information and User Guide for MIL-F-83300, Military Specification-Flying Qualities of Piloted V/STOL Aircraft AFFDL-TR-70-88, Nov. 1970.

11. Stapleford, Robert L.: Analysis of Several Handling Quality Topics Pertinent to Advanced Manned Aircraft: Altitude Control During Approach. AFFDL-TR-67-2, June 1967, pp. 167-204.

12. Ashkenas, I. L.; and Craig, S. J.: Multiloop Piloting Aspects of Longitudinal Approach Path Control. ICAS Paper 72-46, presented at the 8th Congress of International Council of Aeronautical Sciences, Amsterdam, Aug. 28-Sept. 2, 1972, 21 p.

13. Ashkenas, I. L.: Summary and Interpretation of Recent Longitudinal Flying Qualities Results. Journal of Aircraft, vol. 8, no. 5, May 1971, pp. 324-328.

14. Rumsey, P. C.; and Spitzer, R. E.: Simulator Model Specification for the Augmentor Wing Jet STOL Research Aircraft. NASA CR-114434, 1971.

15. Franklin, J. A.; and Koenig, R. W.: A Simulator Investigation of the Influence of Engine Response Characteristics on the Approach and Landing for an Externally Blown Flap Aircraft, Part 1: Description of the Simulation and Discussion of Results. NASA TM X-62,265, 1973.

16. Anderson, R. O.: A New Approach to the Specification and Evaluation of Flying Qualities - Final Report. AFFDL-TR-69-120, Nov. 1969.

17. McRuer, D. T.; Ashkenas, I. L.; and Pass, H. R.: Analysis of Multiloop Vehicular Control Systems. ASD-TDR-62-1014, March 1964.

18. Seckel, Edward: Stability and Control of Airplanes and Helicopters. Academic Press, New York, 1964.

19. Zuccaro, J. J.: The Flight Simulator for Advanced Aircraft - A New Aeronautical Research Tool. AIAA Paper 70-359, March 1970.

20. Quigley, H. C.; Sinclair, S.R.M.; Nark, T. C.; and O'Keefe, J. V.: A Progress Report on the Development of an Augmentor Wing Jet STOL Research Aircraft. SAE Paper 710757, Society of Automotive Engineers, National Aeronautics and Space Engineering and Manufacturing Meeting, Los Angeles, Calif., Sept. 28-30, 1971.

21. Cleveland, W. B.; Vomaske, R. F.; and Sinclair, S.R.M.: Augmentor Wing Jet STOL Research Aircraft Digital Simulation Model. NASA TM X-62,149, 1972.

22. Cooper, George E.; and Harper, Robert P.: The Use of Pilot Rating in the Evaluation of Aircraft Handling Qualities. NASA TN D-5153, 1969.

23. Kelly, James R.; Garren, John F., Jr.; and Deal Perry L.: Flight Investigation of V/STOL Height-Control Requirements for Hovering and Low-Speed Flight Under Visual Conditions. NASA TN D-3977, 1967.

24. Innis, R. C.; Holzhauser, C. A.; and Gallant R. P.: Flight Tests Under IFR With an STOL Transport Aircraft. NASA TN D-4939, 1968.

25. Stapleford, R. L.; Heffley, R. K.; Lehman, J. M.; and Jewell, W. F.: A STOL Airworthiness Investigation Using a Simulation of a Deflected Slipstream Transport, Vol. II: Simulation Data and Analysis. TR 1014-3, Systems Technology, Inc., July 1973.

26. McRuer, Duane T.: Unified Analysis of Linear Feedback Systems. ASD-TR-61-118, July 1961.